



ORIGINAL PAPER

András Szekrényes · Péter Máté · Bence Hauck

On the dynamic stability of delaminated composite beams under free vibration

Received: 18 July 2021 / Revised: 5 February 2022 / Accepted: 21 February 2022 / Published online: 7 April 2022
© The Author(s) 2022

Abstract This work deals with the analysis of the free vibration problem of elastic delaminated composite beams. The work mainly consists of a model development and improvement stage based on the first-order shear deformable beam theory. A general model is developed taking the bending-extensional coupling into account. The specified problem is a built-in beam with free end, and one of the novelties of this work is the consideration of the fact that a built-in beam cannot be fixed rigidly in reality. Thus, a Winkler-type elastic foundation is applied along the built-in length. The total potential energy and the governing equations of the delaminated and intact parts of the beam are also captured. The problem is solved in two ways: analytically and numerically by using the finite element method, respectively. Applying the developed models the natural frequencies, mode shapes as well as the stress resultants are determined. The comparison of natural frequencies to those measured experimentally shows that the built-in length resting on Winkler-type elastic foundation influences significantly the agreement between model and experiment. In the final stage, the parametric excitation phenomenon taking place in the delaminated part is analyzed using a local model and the harmonic balance method. The dynamic buckling is characterized by some stability diagrams, and it is shown that the applied model is very sensitive to the frequency leading to somewhat controversial critical amplitudes compared to measurements.

1 Introduction

One of the main drawbacks of structural composites is—apart from the numerous and obvious advantages—that these materials are susceptible to delamination failure. The delamination or interlaminar fracture alters significantly the dynamic properties of such structural elements. The free vibration analysis of delaminated structures has been investigated since several decades in the literature. The earliest solutions were based on the application of Euler–Bernoulli and Timoshenko beam theories [1–16].

For the free vibration characterization of delaminated beams, the free and constrained mode models were introduced originally in [2]. The free mode model is based on the assumption of independent deflections of the top and bottom subbeams of the delaminated part. This model was found to be physically inconsistent providing interpenetration of the top and bottom subbeams into each other. The constrained mode model, on the other hand, does not make any delamination opening possible during free vibration and leads to a certain stiffening effect compared to the free mode model. In other words, higher stiffness leads to higher frequencies provided that the mass is the same [17].

In the related field, Shen and Grady published an important paper performing vibration measurements and numerical analysis on delaminated beams [18]. They also displayed the mode shapes and showed that the vibration shape is asymmetric during one vibration period. This was obviously an important experimental observation. Later, some more papers were published and the delamination opening was captured by different

approximations [8,9,19]. In [20], nonlinear springs were placed between the crack faces of the top and bottom subbeams. The delamination opening was controlled by the spring stiffness, although only some limit cases were investigated effectively.

The current and recent literature offers large number of works carried out on delaminated composite and sandwich beams under different circumstances. Many authors investigated the problem of multiple delaminated clamped and clamped–clamped beams [16,21–23]. In these papers, the first and second eigenshapes were determined. In a series of articles [24–26], the contact between the delamination faces was modeled and it was concluded that the frequencies decrease with the increase in delamination length. Other authors applied higher-order model analysis [6,27]) and finite element models [28,29] assuming that the delamination opening takes place because of the inertia forces. In [30], experimental results on natural frequency were presented for cross-ply laminated beams using traditional models. In [31], the free vibration of delaminated beams was analyzed considering fluid-structure interaction. The so-called dynamic stiffness method was applied in [32,33] to delaminated composite beams. Moreover, in [34] a delaminated beam subjected to a follower force was analyzed leading to an interesting engineering problem and results. Finally, but not least papers for delamination detection are available as well, e.g.: [35,36]. For sandwich beams with partial delaminations and debonding effect, some recent articles are available, too [37–40]. Models developed for delaminated beams were also extended to plates and shells for the linear and nonlinear vibration analysis by the finite element [41–44] and meshfree [45] methods.

Another important effect is the bending-stretching coupling on the natural frequencies of delaminated beams. Shu and Fan [4] found that the flexural and longitudinal frequencies of Euler–Bernoulli beams are far from each other; therefore, the coupling effect is negligible. Actually, in [20,28] the agreement with the experimental results of Shen and Grady was found to be better by leaving the coupling effect out of consideration. However, in [46] it was elaborated that the former agreement was likely just a fortune: the Euler–Bernoulli theory is inaccurate for the description of the mentioned problem, and the longitudinal wave is influenced by the cross-sectional rotations at the delamination tips. For an accurate model, both the transverse shear effect and longitudinal wave motion are required to be accounted for and if so, then the agreement of the model with the experimental results will be significantly better [46].

To the best of the authors' knowledge, refs. [46,47] were the first publications discovering the existence of parametric excitation during the free vibration of delaminated composite beams. The problem was treated by the method of harmonic balance and the critical forces as well as critical amplitudes were determined numerically and the latter experimentally. The critical force is the value of normal force in the delaminated subbeams which is required to initiate the dynamic buckling during vibration. On the other hand, the critical amplitude is the value of the vibration amplitude at the end of the built-in-free beam that is required to initiate the buckling during the free vibration. These works were followed by a similar analysis of delaminated plates performing free vibration [48]. Since then, several other papers were published; however, in these works the parametric instability was investigated in the traditional way using the harmonic balance [49–51] and the so-called multi-frequency method [17]. In this current work, the main aspect and more specifically the scientific novelty is the application of Winkler elastic foundation, the built-in length is resting on. A general model is developed based on the first-order shear deformable beam theory taking the bending-extension coupling into account. Moreover, the parametric excitation the delaminated part is subjected to is analyzed more deeply than before [47] and it is shown how sensitive the critical buckling force is to the natural frequency.

2 The boundary value problem—strong form

Figure 1 shows the model of a delaminated beam. The beam consists of five parts: (1) and (5) mean the intact part, (3) represents the delaminated part based on the so-called free mode model [2]. Finally, (2) and (4) capture the transition between the intact and delaminated parts of the beam, respectively. The latter is distinctly interpreted from the analytical and finite element modeling points of view. From the analytical viewpoint, regions (2) and (4) mean the continuity conditions between the (1)-(3) and (3)-(5) transitions. From the viewpoint of FE modeling, the continuity between regions (1)-(3) and (3)-(5) is achieved by transition elements (2) and (4), see later. The possible boundary conditions are also shown in Figure 1 and these are: pinned end, built-in (or rigidly fixed) end, intact part resting on elastic (Winkler) foundation and the free end. Any of these can be imposed at both ends of the beam. The related equations will be given later on. Region (0) represents the built-in intact part resting on Winkler-type elastic foundation. It is noteworthy that continuity conditions are required between regions (0)-(1) if the built-in length resting elastic foundation is involved; however, these are straightforward conditions (see later).

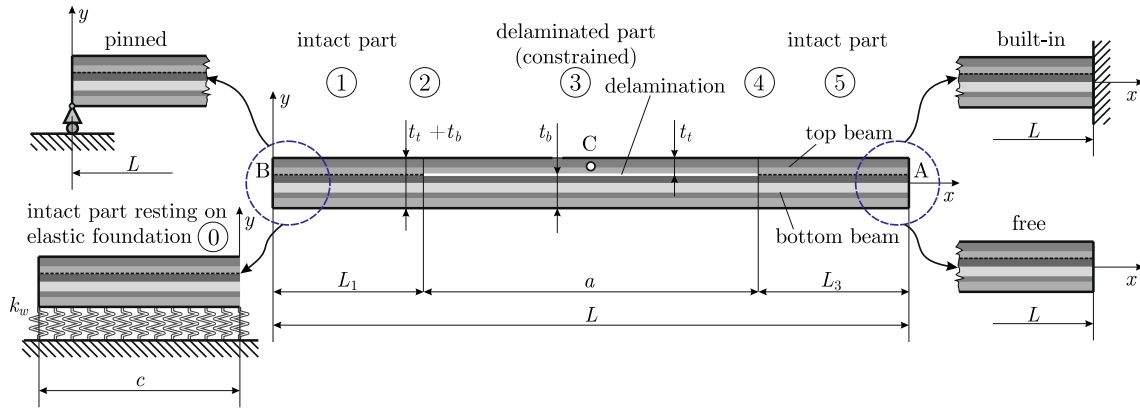


Fig. 1 Mechanical model of a delaminated beam with possible boundary conditions

Each part (1, 2, 3, 4, 5) is further sliced by the plane of the delamination meaning that there are two subbeams in each region: a top (t) and a bottom (b) one, respectively. The kinematic continuity between the top and bottom parts is discussed in the sequel. Each part of the beam is captured by the laminated first-order shear deformable, or simply the Timoshenko beam theory [52]. The assumed displacement field of the model can be written as

$$u_\delta(x, y^{(\delta)}, t) = u_0 + u_\delta^0(x, t) + \theta_\delta(x, t)y^{(\delta)}, \tag{1}$$

where δ can take t or b for the top and bottom subbeams, respectively. Moreover, u_0 is the global membrane displacement, u_δ^0 is the local (through-thickness) constant axial or membrane displacement, θ_δ is the rotation of the cross section about axis z , as it is shown in Fig. 1. In the sequel, the different regions are discussed separately. Figure 2 shows how the transition between regions (1, 2, 3) is established. In Fig. 2a, the two oblique lines separate the intact (1) and delaminated (3) parts, these lines represent the longitudinal displacement distributions and mean that the (1) and (3) portions are described by different mechanical models. These models are connected through the transition(2) by imposing the required continuity conditions. The horizontal lines of the delaminated part (3) are the delamination faces of the top and bottom subbeams. The separation gap between the top and bottom delamination faces is zero. Figure 2b depicts the same transition; however, the top and bottom parts are shown in exploded form. The top and bottom subbeams work perfectly together along the intact part (1) (continuous in-plane displacement), in contrast the delaminated part (3) is discontinuous, meaning that the displacement field of the top and bottom subbeams is independent of each other. The transition between regions (3, 4, 5) is based on the same concept.

2.1 Intact part

Along the intact part, the deflection of the top and bottom beams is the same, i.e.: $v_t(x, t) = v_b(x, t) = v(x, t)$. The in-plane displacements of the top and bottom subbeams at the interface (delamination plane) are identical, i.e., [47]:

$$u_t|_{y^{(t)} = -y_R^{(t)}} = u_b|_{y^{(b)} = t_b - y_R^{(b)}}. \tag{2}$$

The second condition against the in-plane displacements is the assignment of global membrane displacement, u_0 to the reference plane [47]:

$$y_R \begin{cases} \leq t_b : & u_b|_{y^{(b)} = y_R - y_R^{(b)}} = u_0, \\ \geq t_b : & u_t|_{y^{(t)} = -(y_R^{(t)} - y_R + t_b)} = u_0. \end{cases} \tag{3}$$

As it can be seen, two cases are included by Eq.(3): the first case is when the top beam is thinner than the bottom one and obviously the global reference plane is within the bottom subbeam. The second case means that the bottom beam is thinner than the top one and the reference plane is within the top subbeam. Using

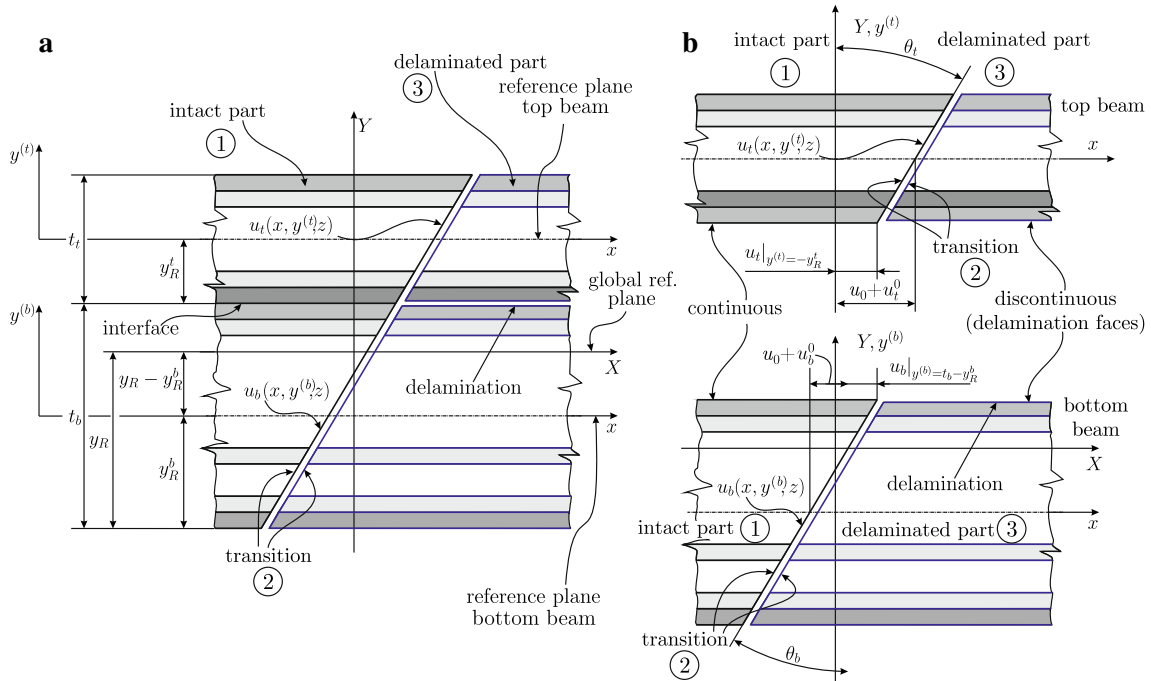


Fig. 2 Reference planes and displacement parameters of the top and bottom subbeams of the intact (1) and delaminated (3) parts, (a). Displacement continuity at transition (2) between the intact (1) and delaminated (3) parts, (b).

Eqs.(2, 3), it is possible to assign the relationship between the constant parts of in-plane displacements and the rotations of the intact part in Eq. (1):

$$u_t^0 = y_R^{(t)} \theta_t + (t_b - y_R) \theta_b, \quad u_b^0 = -(y_R - y_R^{(b)}) \theta_b. \tag{4}$$

Combining Eqs. (1, 2, 3, 4), the displacement functions of the intact part become:

$$u_t = u_0 + y_R^{(t)} \theta_t + (t_b - y_R) \theta_b + \theta_t(x, t) y^{(t)}, \quad u_b = u_0 - (y_R - y_R^{(b)}) \theta_b + \theta_b y^{(b)}. \tag{5}$$

In accordance with the basic equations of linear elasticity [53], the normal strain and shear strain of the top subbeam become:

$$\varepsilon_{xt} = \frac{du_0}{dx} + y_R^{(t)} \frac{d\theta_t}{dx} + (t_b - y_R) \frac{d\theta_b}{dx} + \frac{d\theta_t}{dx} y^{(t)}, \quad \gamma_{xyt} = \frac{dv}{dx} + \theta_t. \tag{6}$$

Likewise, the strains for the bottom subbeam are:

$$\varepsilon_{xb} = \frac{du_0}{dx} - (y_R - y_R^{(b)}) \frac{d\theta_b}{dx} + \frac{d\theta_b}{dx} y^{(b)}, \quad \gamma_{xyb} = \frac{dv}{dx} + \theta_b. \tag{7}$$

To derive the governing equations, we apply Hamilton’s principle [52,53]. Thus, we need the potential energy and the kinetic energy of the system. The former is determined by the following equation:

$$U = \frac{1}{2} \sum_{\delta=t,b} \left(\int_{(V)} \sigma_{ij(\delta)} \varepsilon_{ij(\delta)} dV \right) = \frac{1}{2} \sum_{\delta=t,b} \left(\int_{(V)} (\sigma_{x(\delta)} \varepsilon_{x(\delta)} + \tau_{xy(\delta)} \gamma_{xy(\delta)}) dV \right), \tag{8}$$

which is the sum of volumetric integrals for the top and bottom subbeams. Calculating the stresses using the constitutive equation and carrying out the surface integral to the beam cross section, we have

$$U = \frac{1}{2} \sum_{\delta=t,b} \left(\int_{(L)} (N_{x(\delta)} \varepsilon_x^0(\delta) + M_{x(\delta)} \varepsilon_x^1(\delta) + Q_{x(\delta)} \gamma_{xy(\delta)}) dx \right), \tag{9}$$

where L is the length, N_x is the normal force, M_x is the bending moment, Q_x is the shear force, i.e., the stress resultants, that are determined by [52,54]:

$$\begin{pmatrix} N_x \\ M_x \end{pmatrix}_\delta = \begin{pmatrix} A_{11} & B_{11} \\ B_{11} & D_{11} \end{pmatrix}_\delta \begin{pmatrix} \varepsilon_{y\delta}^0 \\ \varepsilon_{x\delta}^1 \end{pmatrix}_\delta, \quad Q_{x\delta} = kA_{55\delta}\gamma_{xy\delta}, \tag{10}$$

where A_{11} , B_{11} , D_{11} and A_{55} are the extensional, coupling, bending and shear stiffnesses computed based on the lay-up of the beam and each is determined with respect to the local midplane of the actual subbeam:

$$(A_{11}, B_{11}, D_{11})_\delta = \sum_{k=1..N} \int_{y_k^{(\delta)}}^{y_{k+1}^{(\delta)}} bE_{11}^{(k)}(1, y, y^2)dy^{(\delta)}, \quad A_{55\delta} = k \sum_{l=1..N} \int_{y_l^{(\delta)}}^{y_{l+1}^{(\delta)}} bG_{12}^{(l)}dy^{(\delta)}, \tag{11}$$

where E_{11} is the flexural, G_{12} is the shear modulus, b is the width and $k = 5/6$ is the shear correction factor for rectangular cross section, respectively.

We continue with the determination of the kinetic energy of the beam. Similarly to the potential one, the kinetic energy is calculated by summing the relevant expressions to the top and bottom subbeams:

$$\mathcal{T} = \frac{1}{2} \sum_{\delta=t,b} \left(\int_{(V)} \rho_{(\delta)} \dot{u}_{i(\delta)} \dot{u}_{i(\delta)} dV \right) = \frac{1}{2} \sum_{\delta=t,b} \left(\int_{(V)} \rho (u_{(\delta)}^0)^2 + 2\dot{u}_{(\delta)}^0 \dot{\theta}_\delta y^\delta + (\dot{\theta}_\delta y^\delta)^2 dV \right). \tag{12}$$

Considering the fact that the density, ρ , may vary from layer-by-layer, after integrating Eq. (12) with respect to the cross-sectional surface we can write the following:

$$\mathcal{T} = \frac{1}{2} \int_{(L)} (I_{0\delta}(\dot{u}_{(\delta)}^0)^2 + 2I_{1\delta}\dot{u}_{(\delta)}^0 \dot{\theta}_\delta + I_{2\delta}\dot{\theta}_\delta^2) dx, \tag{13}$$

where the so-called inertia parameters [52] are defined by:

$$I_0, I_1, I_2 = \sum_{k=1..N} \int_{y_k^{(\delta)}}^{y_{k+1}^{(\delta)}} b\rho^{(k)}(1, y, y^2)dy^{(\delta)}. \tag{14}$$

The variational calculus is performed to obtain the governing equations of the system. The variation of the total potential energy, $\Pi = \mathcal{U} - \mathcal{T}$, with respect to the global membrane displacement provides the following equation:

$$\begin{aligned} \delta u_0 : N_{xt,x} + N_{xb,x} &= (I_{0t} + I_{0b})\ddot{u}_0 + I_{0t}(y_{Rt}\ddot{\theta}_t + (t_b - y_R)\ddot{\theta}_b) \\ &\quad - I_{0b}(y_R - y_{Rb})\ddot{\theta}_b + I_{1t}\ddot{\theta}_t + I_{1b}\ddot{\theta}_b. \end{aligned} \tag{15}$$

The variation with respect to the rotations leads to further two equations:

$$\begin{aligned} \delta \theta_t : M_{xt,x} + y_{Rt}N_{xt,x} - Q_{xt} \\ &= (I_{0t}y_{Rt} + I_{1t})\ddot{u}_0 + (I_{0t}y_{Rt}^2 + I_{1t}2y_{Rt} + I_{2t})\ddot{\theta}_t \\ &\quad + (I_{0t}y_{Rt} + I_{1t})(t_b - y_R)\ddot{\theta}_b, \end{aligned} \tag{16}$$

$$\begin{aligned} \delta \theta_b : M_{xb,x} - (y_R - y_{Rb})N_{xb,x} + (t_b - y_R)N_{xt,x} - Q_{xb} \\ &= (I_{0t}(t_b - y_R) - I_{0b}(y_R - y_{Rb}) + I_{1b})\ddot{u}_0 \\ &\quad + (I_{0t}y_{Rt}(t_b - y_R) + I_{1t}(t_b - y_R))\ddot{\theta}_t \\ &\quad + (I_{2b} + I_{0t}(t_b - y_R)^2 + I_{0b}(y_R - y_{Rb})^2)\ddot{\theta}_b \\ &\quad + -2I_{1b}(y_R - y_{Rb})\ddot{\theta}_b. \end{aligned} \tag{17}$$

Finally, the equation with respect to the transverse deflection (or vibration) becomes:

$$\delta v : Q_{xt,x} + Q_{xb,x} = (I_{0t} + I_{0b})\ddot{v}. \tag{18}$$

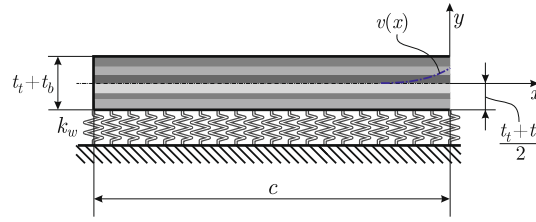


Fig. 3 Elastic foundation part (0) with parameters required to determine the k_w foundation stiffness

2.2 Delaminated part—free mode model

The delaminated part is modeled by traditional laminated first-order shear deformable (Timoshenko) beams; both the top and bottom subbeams are based on Eq.(1); however, u_0 is ignored. The procedure to obtain the governing equations is exactly the same as it was in the case of the intact part. The most important aspect is that independent membrane displacements, rotations and deflections are implied. The latter means that a free mode model is applied. The governing equations obtained based on variational calculus are:

$$\delta u_{0\delta} : N_{x(\delta),x} = I_{0\delta} \ddot{u}_{0\delta} + I_{1\delta} \ddot{\theta}_{x\delta}, \tag{19}$$

$$\delta \theta_{\delta} : M_{x(\delta),x} - Q_{x(\delta)} = I_{1\delta} \ddot{u}_{0\delta} + I_{2\delta} \ddot{\theta}_{x\delta}, \tag{20}$$

$$\delta v_{\delta} : Q_{x(\delta),x} = I_{0\delta} \ddot{v}_{\delta}. \tag{21}$$

where Eqs.(19, 20, 21) are related to the longitudinal, rotational and transverse wave motion including the coupling effect.

2.3 Elastic foundation part

If any of the beam ends is extended by a built-in length resting on Winkler-type foundation, then the first step is that we determine the foundation stiffness (k_w). This stiffness should be determined in terms of the through-thickness modulus based on Fig. 3 and the following equations [55]:

$$k_w = \frac{b\sigma_y(x)}{v(x)}, \quad \sigma_y(x) = E_{22}\varepsilon_y(x), \quad \varepsilon_y(x) = \frac{v(x)}{(t_t + t_b)/2}. \tag{22}$$

where σ_y is the average transverse normal stress in the beam and determined by the simple Hooke’s law by the second equation. Moreover, ε_y is the through-thickness strain. In accordance with Fig. 3, the strain is calculated by the ratio of change of original length over the original length in the transverse direction. The combination of the equations above leads to the following result:

$$k_w = \frac{b}{t_t + t_b} E_{22}. \tag{23}$$

The basic concept of the built-in part resting on Winkler foundation (refer to Fig. 1) is that is far enough from the delamination tip, and thus, there is no need to imply two independent rotations of the top and bottom subbeams. Thus, the potential and kinetic energies of the system can be derived in the standard way. The only difference is that the springs should be considered. The elastic energy stored in the foundation springs is given by:

$$\mathcal{U}_w = \frac{1}{2} \int_{(c)} k_w v_b^2 dx, \tag{24}$$

The governing equations based on variational calculus become:

$$\delta u_0 : N_{x,x} = I_0 \ddot{u}_0 + I_1 \ddot{\theta}_x, \tag{25}$$

$$\delta \theta_x : M_{x,x} - Q_x = I_1 \ddot{u}_0 + I_2 \ddot{\theta}_x, \tag{26}$$

$$\delta v : Q_{x,x} - k_w v = I_0 \ddot{v}, \tag{27}$$

describing again the longitudinal, rotational and transverse wave motions together with the coupling effect.

Table 1 Continuity conditions of the delaminated composite beam in Fig. 1

Description	Conditions
Displacement and rotation	$V_1(L_1) = V_{2l}(L_1)$ $X_{r1}(L_1) = X_{r2}(L_1)$
	$V_1(L_1) = V_{2b}(L_1)$ $X_{b1}(L_1) = X_{b2}(L_1)$
	$V_3(L_1 + a) = V_{2l}(L_1 + a)$ $X_{r1}(L_1 + a) = X_{r2}(L_1 + a)$
	$V_3(L_1 + a) = V_{2b}(L_1 + a)$ $X_{b1}(L_1 + a) = X_{b2}(L_1 + a)$
Longitudinal displacement	$(U_{01} + y_R^{(l)} X_{r1} + (t_b - y_R) X_{b1}) _{x=L_1} = U_{02l}(L_1)$
	$(U_{01} - (y_R - y_R^{(b)}) X_{b1}) _{x=L_1} = U_{02b}(L_1)$
	$(U_{03} + y_R^{(l)} X_{r3} + (t_b - y_R) X_{b3}) _{x=L_1+a} = U_{02l}(L_1 + a)$
Equivalent bending moment	$(U_{03} - (y_R - y_R^{(b)}) X_{b3}) _{x=L_1+a} = U_{02b}(L_1 + a)$
	$\hat{M}_{xt1}(L_1) + \hat{M}_{xb1}(L_1) = \hat{M}_{xt2}(L_1) + \hat{M}_{xb2}(L_1)$
Shear forces	$(\hat{M}_{xt2} + \hat{M}_{xb2}) _{x=a+L_1} = (\hat{M}_{xt3} + \hat{M}_{xb3}) _{x=a+L_1}$
	$Q_{xt1}(L_1) = Q_{xt2}(L_1), Q_{xb1}(L_1) = Q_{xb2}(L_1)$
Normal forces	$Q_{xt2}(a + L_1) = Q_{xt3}(a + L_1), Q_{xb2}(a + L_1) = Q_{xb3}(a + L_1)$
	$(N_{xt1} + N_{xb1}) _{x=L_1} = (N_{xb2} + N_{xt2}) _{x=L_1}$
	$(N_{xt3} + N_{xb3}) _{x=a+L_1} = (N_{xb2} + N_{xt2}) _{x=a+L_1}$

Table 2 Boundary conditions of the delaminated composite beam depending on the constraints in Fig. 1

Description	Conditions
End with elastic foundation	$M_{x0}(-c) = 0$ $N_{x0}(-c) = 0, Q_{x0}(-c) = 0$
	$V_1(0) = V_0(0), U_{01}(0) = U_{00}(0)$ $X_{r1}(0) = X_0(0), X_{b1}(0) = X_0(0)$
Free end	$\hat{M}_{xt3}(L) = 0, \hat{M}_{xb3}(L) = 0$ $(Q_{xt3} + Q_{xb3}) _{x=L} = 0, (N_{xt3} + N_{xb3}) _{x=L} = 0$
Pinned end	$\hat{M}_{xt1}(0) = 0, \hat{M}_{xb1}(0) = 0$ $V_3(0) = 0, (N_{xt1} + N_{xb1}) _{x=L} = 0$
Built-in end	$U_{03}(L) = 0, V_3(L) = 0$ $X_{r3}(L) = 0, X_{b3}(L) = 0$

2.4 Frequency and mode shape analysis

The system of governing equations (15, 16, 17, 18), (19, 20, 21) and (25, 26, 27) can be solved easily for each region of the beam for example based on the previous works of the author [46,47]. For any regions of the beam, the deflection and the rotations can be obtained by assuming harmonic motion in time:

$$\begin{pmatrix} v_\delta(x, t) \\ \theta_\delta(x, t) \\ u_{0\delta}(x, t) \end{pmatrix} = \begin{pmatrix} V_\delta(x) \\ X_\delta(x) \\ U_{0\delta}(x) \end{pmatrix} \sin(\alpha t), \quad \begin{pmatrix} V_\delta(x) \\ X_\delta(x) \\ U_{0\delta}(x) \end{pmatrix} = \begin{pmatrix} K_\delta \\ L_\delta \\ M_\delta \end{pmatrix} e^{\lambda x}, \tag{28}$$

where α is the natural frequency of the system and λ is the characteristic root. Moreover, $V_\delta(x), U_\delta(x)$ and $\theta_\delta(x)$ are the eigenshape functions of the corresponding parameters representing the standing wave solution of the free vibration problem.

The required continuity conditions are listed in Table 1. The set of conditions includes the continuity of displacement parameters and the sum of stress resultants at the transitions. The conditions against the longitudinal displacements are derived based on Eq.(5). An important detail is that between (1)-(3) and (3)-(5) the equivalent bending moments should be used to ensure the continuity [46], these are derived based on Eqs.(16, 17):

$$\hat{M}_{xt} = M_{xt} + y_{Rl} N_{xt}, \quad \hat{M}_{xb} = M_{xb} - (y_R - y_{Rb}) N_{xb} + (t_b - y_R) N_{xt}. \tag{29}$$

The possible boundary conditions shown in Fig. 1 are formulated by equations in Table 2. If the ends are resting on elastic foundation, then further continuity conditions are required between regions (0) and (1).

Based on the solution functions, boundary and continuity conditions, a system of linear algebraic equations is created and the determinant of the matrix term provides the frequency equation. The latter can be solved by, e.g., a bisection method [17,50] to find the natural frequencies of the system. In the knowledge of the frequencies, the eigenshapes in Eq.(28) can be determined by using the system of algebraic equations and determining the constant coefficients (K, L and M).

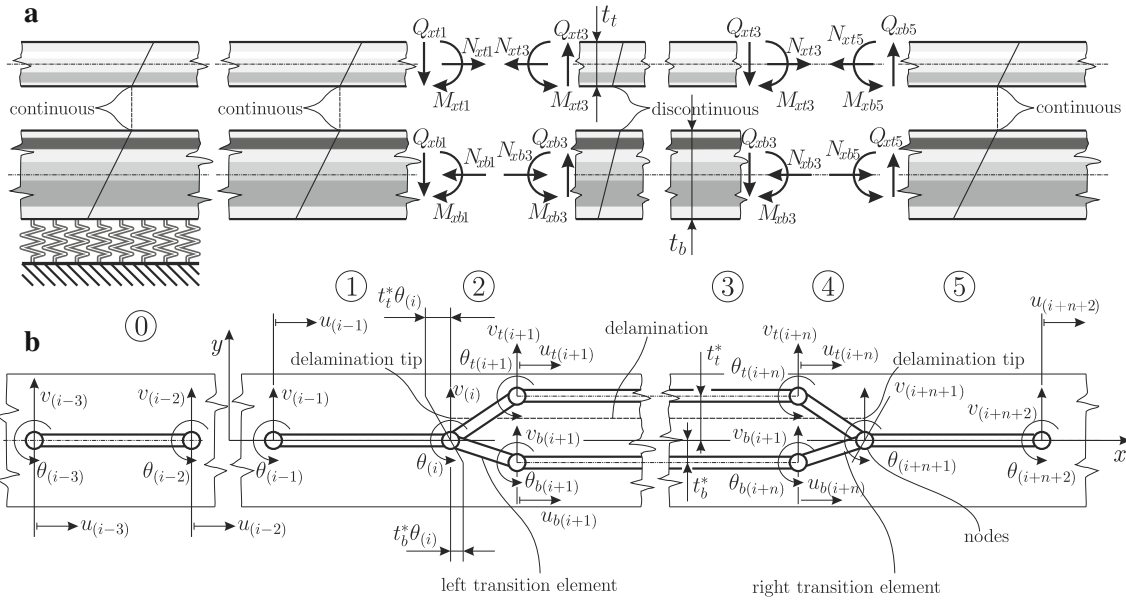


Fig. 4 Stress resultants at the transition cross sections of a delaminated composite beam (a). Finite element discretization and nodal DoFs of a composite beam with delamination (b).

3 Finite element discretization—weak form

The finite element discretization is carried out based on the weak formulation of the problem [52,56]. The FE model is developed based on Fig. 4 indicating the stress resultants (a) and the nodal parameters (b). Essentially, for each region—shown by Fig. 4b—there are three independent displacement parameters: the membrane displacement, the rotation and the deflection. The interpolation scheme of these parameters is the following:

$$u_0 = \mathbf{N}_u^T \mathbf{u}_e, \theta = \mathbf{N}_\theta^T \mathbf{u}_e, v = \mathbf{N}_v^T \mathbf{u}_e, \tag{30}$$

where \mathbf{N}_u , \mathbf{N}_θ and \mathbf{N}_v are the vectors of interpolation functions and contain the linear, quadratic and cubic interpolation functions, respectively [57].

3.1 Elastic foundation part

We get started with the elastic foundation part (region (0) in Fig. 4) and based on Eq. (9) it is possible to give the potential energy of the system by:

$$\mathcal{U} = \frac{1}{2} \mathbf{u}_e^T (\mathbf{K}_{eu} + \mathbf{K}_{eu\theta} + \mathbf{K}_{e\theta} + \mathbf{K}_{esh} + \mathbf{K}_{ew}) \mathbf{u}_e, \tag{31}$$

where the stiffness matrices are defined as:

$$\mathbf{K}_{eu} = \int_0^1 \frac{\beta_1}{l_e} \mathbf{N}'_u \mathbf{N}'_u{}^T d\xi, \quad \mathbf{K}_{eu\theta} = \int_0^1 \frac{\beta_2}{l_e} (\mathbf{N}'_u \mathbf{N}'_\theta{}^T)_{\text{sym}} d\xi, \quad \mathbf{K}_{e\theta} = \int_0^1 \frac{\beta_3}{l_e} \mathbf{N}'_\theta \mathbf{N}'_\theta{}^T d\xi, \tag{32}$$

where ξ is the dimensionless coordinate and l_e is the element length. Note that in the middle of Eq. (32) the symmetric part of the product should be determined. Moreover:

$$\mathbf{K}_{esh} = \int_0^1 \beta_4 \mathbf{B}_{sh} \mathbf{B}_{sh}^T l_e d\xi, \quad \mathbf{K}_{ew} = \int_0^1 k_w \mathbf{N}_v \mathbf{N}_v^T l_e d\xi, \tag{33}$$

where β denotes coefficients related to the stiffness parameters, \mathbf{B} is the strain-displacement vector:

$$\beta_1 = A_{11t} + A_{11b}, \quad \mathbf{B}_{sh} = \mathbf{N}_\theta + \frac{1}{l_e} \mathbf{N}'_v, \tag{34}$$

$$\beta_2 = 2A_{11t}(y_{Rt} + t_b - y_R) - 2A_{11b}(y_R - y_{Rb}) + 2(B_{11t} + B_{11b}), \tag{35}$$

$$\beta_3 = A_{11t}(y_{Rt}^2 + (t_b - y_R)^2) - A_{11b}(y_R - y_{Rb})^2 + 2B_{11t}(y_{Rt} + t_b - y_R) - 2B_{11b}(y_R - y_{Rb}) + D_{11t} + D_{11b}, \tag{36}$$

$$\beta_4 = k(A_{55t} + A_{55b}). \tag{37}$$

The kinetic energy of the system can be formulated based on Eqs. (13)–(14). The following can be obtained:

$$\mathcal{T} = \frac{1}{2} \dot{\mathbf{u}}_e^T (\mathbf{M}_{eu} + \mathbf{M}_{eu\theta} + \mathbf{M}_{e\theta} + \mathbf{M}_{ev}) \dot{\mathbf{u}}_e, \tag{38}$$

where the mass matrices are given below:

$$\mathbf{M}_{eu} = \int_0^1 \kappa_1 \mathbf{N}_u \mathbf{N}_u^T l_e d\xi, \quad \mathbf{M}_{eu\theta} = \int_0^1 \kappa_2 (\mathbf{N}'_u \mathbf{N}'_\theta^T)_{\text{sym}} l_e d\xi, \tag{39}$$

$$\mathbf{M}_{e\theta} = \int_0^1 \kappa_3 \mathbf{N}_\theta \mathbf{N}_\theta^T l_e d\xi, \quad \mathbf{M}_{ev} = \int_0^1 \kappa_1 \mathbf{N}_v \mathbf{N}_v^T l_e d\xi. \tag{40}$$

The coefficients, denoted by κ , are related to the inertia parameters according to the following:

$$\kappa_1 = I_{0t} + I_{0b}, \tag{41}$$

$$\kappa_2 = 2I_{0t}(y_{Rt} + t_b - y_R) - 2I_{0b}(y_R - y_{Rb}) + 2(I_{1t} + I_{1b}), \tag{42}$$

$$\kappa_3 = I_{0t}(y_{Rt}^2 + (t_b - y_R)^2) + I_{0b}(y_R - y_{Rb})^2 + 2I_{1t}(y_{Rt} + t_b - y_R) - 2I_{1b}(y_R - y_{Rb}) + I_{2t} + I_{2b}. \tag{43}$$

To calculate the vectors of interpolation functions, we assign the function approximation as follows:

$$v_e = \sum_{i=0}^3 a_i \xi_i, \quad \theta_e = \gamma_{0e} - \frac{1}{l_e} v'_e, \quad u_e = \sum_{i=0}^1 b_i \xi_i \tag{44}$$

where γ_{0e} is the shear strain. The literature offers different variants of the interpolation of Timoshenko beams [58], in this work an element with constant elementwise shear strain is chosen [52,56]. The shear strain can be determined based on the static equilibrium equation of the intact part, i.e., by Eqs. (16, 17) and assuming identical rotations ($\theta_b = \theta_t$):

$$\gamma_{0e} = \frac{6a_3\beta_3}{l_e^3(A_{55t} + A_{55b})}. \tag{45}$$

The a_i and b_i coefficients in Eq. (44) can be determined based on the nodal conditions. Since this is a standard FE step [47,52,56], it is not detailed in this paper. The vector of nodal displacements of the intact part with elastic foundation becomes (refer to Fig. 4b):

$$\mathbf{u}_e^T = (u_1 \ v_1 \ \theta_1 \ u_2 \ v_2 \ \theta_2). \tag{46}$$

Using the above and the interpolated forms by Eq. (30), it is possible to seek the interpolation functions and the corresponding vectors. Afterward, the stiffness and mass matrices can be determined as well.

3.2 The intact part

Out of the stiffness matrices in Eq. (31), \mathbf{K}_{ew} should be ignored to have the total stiffness matrix of the intact part denoted by (1) in Fig. 1. The mass matrices are the same as given by Eqs. (39, 40). It is important to note that in the FE model the rotations are the same in the top and bottom subbeams of the intact part, in contrast with the analytical model (refer to Eq. (15)). The comparison of the analytical and FE models indicated that the two different cases lead to essentially the same natural frequencies and mode shapes.

3.3 Transition elements

The left transition element denoted by (2) can be seen in Fig. 4b and provides the kinematic relationship (continuity) between the intact (1) and delaminated (3) parts. In other words, the transition element represents the delamination tip. As it can be recognized, there is one node at the left side and two nodes are on the right-hand side. Thus, the nine related DoFs and the vector of nodal displacements can be written as:

$$\mathbf{u}_e^T = (u_1 \ v_1 \ \theta_1 \ u_{t2} \ v_{t2} \ \theta_{t2} \ u_{b2} \ v_{b2} \ \theta_{b2}). \quad (47)$$

The displacement parameters are interpolated by the following scheme:

$$\begin{Bmatrix} u_t(\xi) \\ v_t(\xi) \\ \theta_t(\xi) \\ u_b(\xi) \\ v_b(\xi) \\ \theta_b(\xi) \end{Bmatrix} = \sum_{i=1}^9 \begin{Bmatrix} N_{ui}^t \\ N_{vi}^t \\ N_{\theta i}^t \\ N_{ui}^b \\ N_{vi}^b \\ N_{\theta i}^b \end{Bmatrix} u_{ei}, \quad (48)$$

where the displacement parameters are captured by:

$$u_\delta(\xi) = \sum_{i=0}^1 b_{i\delta} \xi^i = \sum_{i=1}^9 N_{ui}^\delta u_i = (\mathbf{N}_u^\delta)^T \mathbf{u}_e, \quad (49)$$

$$v_\delta(\xi) = \sum_{i=0}^3 a_{i\delta} \xi^i = \sum_{i=1}^9 N_{vi}^\delta u_i = (\mathbf{N}_v^\delta)^T \mathbf{u}_e, \quad (50)$$

$$\theta_{\delta e}(\xi) = \gamma_{0\delta e} - \frac{1}{l_e} \frac{dv_{\delta e}}{d\xi} = (\mathbf{N}_\theta^\delta)^T \mathbf{u}_e, \quad \gamma_{0\delta e} = \frac{6D_{11\delta} a_{3\delta}}{l_e^2 A_{55\delta}}, \quad (51)$$

where γ_0 is determined again based on the static equilibrium equation (set the right hand side of Eq. (20) to zero) and the elementwise constant shear strain assumption for the static case. The deflection and the angle of rotation is formulated quite similarly; however, the deflection is approximated by cubic, the rotation is interpolated by quadratic functions, and the latter two are not independent of each other (refer to Eq. (34)). The equations above mean twelve unknown coefficients altogether. The required nodal conditions in accordance with Fig. 4b and Eq. (5) are:

$$\begin{aligned} v_t(0) &= v_1, & v_t(1) &= v_{t2}, & \theta_t(0) &= \theta_1, & \theta_t(1) &= \theta_{t2}, \\ v_b(0) &= v_1, & v_b(1) &= v_{b2}, & \theta_b(0) &= \theta_1, & \theta_b(1) &= \theta_{b2}, \end{aligned} \quad (52)$$

$$\begin{aligned} u_t(0) &= u_1 + (y_R^{(t)} + t_b - y_R)\theta_1, & u_t(1) &= u_{t2}, \\ u_b(0) &= u_1 - (y_R - y_R^{(b)})\theta_1, & u_b(1) &= u_{b2}. \end{aligned} \quad (53)$$

With the aid of the conditions above, the vectors of interpolation functions and the stiffness matrices can be determined exactly in the same way as it was performed for the intact part, i.e., using Eqs. (31, 32, 33, 34, 35, 36, 37). Thus, the stiffness matrices of the left transition element are:

$$\mathbf{K}_{eu} = \sum_{\delta=t}^b \int_0^1 \frac{A_{11\delta}}{l_e} \mathbf{N}'_{u\delta} \mathbf{N}'_{u\delta T} d\xi, \quad \mathbf{K}_{e\theta} = \sum_{\delta=t}^b \int_0^1 \frac{2B_{11\delta}}{l_e} (\mathbf{N}'_{u\delta} \mathbf{N}'_{\theta\delta T})_{\text{sym}} d\xi, \quad (54)$$

and:

$$\mathbf{K}_{esh} = \sum_{\delta=t}^b \int_0^1 A_{55\delta} l_e \mathbf{B}_{sh\delta} \mathbf{B}_{sh\delta}^T d\xi, \quad \mathbf{K}_{e\theta} = \sum_{\delta=t}^b \int_0^1 \frac{D_{11\delta}}{l_e} \mathbf{N}'_{\theta\delta} \mathbf{N}'_{\theta\delta T} d\xi, \quad (55)$$

where:

$$\mathbf{B}_{sh\delta} = \mathbf{N}_{\theta\delta} + \frac{1}{l_e} \mathbf{N}'_{v\delta}, \tag{56}$$

Using the kinetic energy expression by Eq. (13) and the vectors of interpolation functions in Eq. (49, 50, 51), the mass matrices are calculated as:

$$\mathbf{M}_{eu} = \sum_{\delta=t}^b \int_0^1 I_{0\delta} \mathbf{N}_{u\delta} \mathbf{N}_{u\delta}^T l_e d\xi, \quad \mathbf{M}_{eu\theta} = \sum_{\delta=t}^b \int_0^1 2I_{1\delta} (\mathbf{N}_{u\delta} \mathbf{N}_{\theta\delta}^T)_{\text{sym}} l_e d\xi, \tag{57}$$

$$\mathbf{M}_{e\theta} = \sum_{\delta=t}^b \int_0^1 I_{1\delta} \mathbf{N}_{\theta\delta} \mathbf{N}_{\theta\delta}^T l_e d\xi, \quad \mathbf{M}_{ev} = \sum_{\delta=t}^b \int_0^1 I_{0\delta} \mathbf{N}_{v\delta} \mathbf{N}_{v\delta}^T l_e d\xi. \tag{58}$$

The right transition element is also visible in Fig. 4b and by means of the previous procedure the stiffness and mass matrices can be derived similarly.

3.4 Delaminated part

The FE matrices of the delaminated part can be obtained quite simply in the knowledge of the previous computations. The laminated Timoshenko beam element with elementwise constant shear strain is applied to both the top and bottom subbeams [59]. Moreover, in Eqs. (32, 33) and in Eqs. (39, 40) the following parameters should be altered (obviously, there is no elastic foundation):

$$\beta_1 = A_{11\delta}, \quad \beta_2 = 2B_{11\delta}, \quad \beta_3 = D_{11\delta}, \quad \beta_4 = kA_{55\delta}, \tag{59}$$

$$\kappa_1 = I_{0\delta}, \quad \kappa_2 = 2I_{1\delta}, \quad \kappa_3 = I_{2\delta}, \tag{60}$$

where the matrices should be determined equally for the top and bottom subbeams. The interpolation scheme is quite similar to that by Eq. (44).

3.5 Boundary conditions

The possible boundary conditions of the FE model are discussed based on Fig. 1. If the boundary is pinned, then the end section is constrained by fixing the deflection and the longitudinal displacement at that node. For a built-in end the deflection, membrane displacement and the rotation are equally zero. If the end is free, then there is nothing to do with that since only the kinematic conditions are treated by the FE method [56].

3.6 Free mode model with no delamination opening

In a recent paper [47], it was shown that for beams made out of unidirectional layers, i.e., when the material is transversely isotropic, then the free mode model can be modified in order to prevent the delamination opening during vibration. Let $\eta = t_t/t_b$ be the ratio of thicknesses, then the modified densities satisfying the conservation law of mass become [47]:

$$\rho_{eq}^{(t)} = \rho \frac{(1 + \eta)\eta^2}{1 + \eta^3}, \quad \rho_{eq}^{(b)} = \rho(1 + \eta) - \rho_{eq}^{(t)}\eta. \tag{61}$$

In accordance with the equations above, the densities and so the inertia parameters in the top and bottom subbeams of the delaminated part (3) should be modified. In some recent papers [46,47], it has been shown that these equations work perfectly in transversely isotropic beams including the Euler–Bernoulli and Timoshenko beam theories as well. However, if the system is discretized by the FE method, then the equations above work correctly only for the Euler–Bernoulli beam theory, but not for the Timoshenko beam element. The reason is the elementwise constant strain approximation. In spite of that, by introducing a further power parameter in the equations of the inertia parameters the delamination opening can be prevented:

$$I_{0t} = \rho_{eq}^{(t)} b t_t (1 + (t_t/t_b))^{p_0}, \quad I_{0b} = \rho b (t_t + t_b) - I_{0t}, \tag{62}$$

Table 3 Reference plane coordinates for unidirectional isotropic beams with symmetric lay-up

y_R	y_{Rt}	y_{Rb}
$(t_t + t_b)/2$	$t_t/2$	$t_b/2$

Table 4 Geometry of the tested delaminated composite beams

a [mm]	60	80	100	120
L_1 [mm]	58	46	33	24
L_3 [mm]	62	54	47	36

where p_0 is the power parameter and its value depends on the position and the length of delamination. In other words, it should be determined by a trial or iterative technique calculating the mode shapes and observing the delamination opening relatively to the vibration amplitude. The natural frequencies are not influenced by the power parameter, because the vibrating mass is always the same. The power parameters will be given later (refer to Table 5).

3.7 Free vibration analysis

The free vibration analysis of the system was carried out in the usual way by solving the $\mathbf{M}\ddot{\mathbf{U}} + \mathbf{K}\mathbf{U} = \mathbf{0}$ equation of motion by assuming harmonic motion in time: $\mathbf{U} = \mathbf{A} \sin \alpha t$, where α is the natural frequency of the system. The first step is to determine the natural frequencies through the $\det(-\alpha^2 \mathbf{M} + \mathbf{K}) = 0$ equation, then by using the frequencies the second step involves the calculation of the eigenshape vectors by means of the $(-\alpha^2 \mathbf{M} + \mathbf{K})\mathbf{U} = \mathbf{0}$ equation. Note that damping is not considered in the analysis; however, a recent publication [50] revealed that the effect of damping on the natural frequencies is negligible from engineering point of view.

4 Geometry, material properties and ANSYS plane FE model

The analysis is carried out on delaminated composite beams made out of unidirectional glass-polyester layers. The left end is resting on elastic foundation, the right end is free in accordance with Fig. 1. This model is referred to as “elastic.” For comparison purposes, the left end is built-in and the analysis is carried out again, the model is referred to as “rigid.” The properties required for the analysis are: $E_{11}=33$ GPa, $E_{22}=7.2$ GPa, $G_{12}=3$ GPa, $\rho=1330$ kg/m³, $L=180$ mm (total length), $c=50$ mm (built-in length), $b=20$ mm (width). The thickness of the beams is always 6.2 mm ($=t_t + t_b$). The reference plane coordinates in this special case are listed in Table 3. The length of delamination, a as well as L_1 and L_3 are given in Table 4. Each beam is built-up using 14 unidirectional layers. The primal assembly of the system is performed based on Fig. 4b. In the sequel, a user-defined beam code number will be assigned to refer to the delamination length and the thicknesswise position of the delamination: as matter of fact, the 60/0 code means that the length of delamination is 60 mm (first number) and the position of the delamination is exactly the global midplane of the beam (second number), i.e.: $t_t = t_b = 6.2 \cdot 7/14 = 3.1$ mm. Some other code numbers are: 60/2 meaning that the thicknesses are: $t_t = 6.2 \cdot 5/14$ mm and $t_b = 6.2 \cdot 9/14$ mm, 60/4 means that $t_t = 6.2 \cdot 3/14$ mm and $t_b = 6.2 \cdot 11/14$ mm, finally 60/6 means that $t_t = 6.2 \cdot 1/14$ mm and $t_b = 6.2 \cdot 13/14$ mm. The number of elements is chosen to achieve the convergence of the first four natural frequencies. For the 60/... and 80/... beams, $N_{e0} = N_{e1} = N_{e3} = N_{e5} = 30$ elements are applied. In the case of the 100/... and 120/... beams, $N_{e0} = 30$, $N_{e1} = N_{e5} = 20$ and $N_{e3} = 40$ elements are used. The lengths of the transition elements are $L_2 = L_4 = 0.5$ mm. The power parameters for the specified geometries are given in Table 5.

To validate the results of the analytical and the own-developed FE models, the delaminated beams with $c=50$ mm long built-in length and free end are created in ANSYS, too, using isoparametric QUAD elements under plane stress assumption. The element size is 1 mm \times 1 mm in each case, and the convergence of the frequencies is checked. Mode shapes are also determined, and the delamination opening is prevented by imposing identical transverse displacements along the nodes of the two delamination faces. The mode shapes are physically consistent with those obtained by the analytical and own-developed FE solutions.

Table 5 Power parameter for the Timoshenko beam finite element for Eq.(62)

Beam code	60/0	60/2	60/4	60/6	80/0	80/2	80/4	80/6
p_0	0	3.52	0.91	0.28	0	4.40	1.40	0.52
Beam code	100/0	100/2	100/4	100/6	100/0	100/2	100/4	100/6
p_0	0	5.25	1.74	0.74	0	4.40	1.40	0.52

Table 6 Free vibration frequencies of the (60/0) and (60/2) composite beams with built-in+free ends in [Hz]

Beam configuration	60/0				60/2			
	f_1	f_2	f_3	f_4	f_1	f_2	f_3	f_4
Modal hammer test	133	855	1824	3900	134	875	1881	4005
Sweep excitation test	128	858	1918	3962	124	826	1908	3992
E.-B., rigid, analytical	152	961	2025	4566	153	965	2153	4749
E.-B., rigid, FEM	152	960	2025	4567	153	964	2153	4750
E.-B., elastic, analytical	141	897	1901	4297	142	899	2019	4451
E.-B., elastic, FEM	141	896	1901	4301	142	898	2019	4455
Timoshenko, rigid, analytical	151	941	1966	4291	152	944	2083	4436
Timoshenko, rigid, FEM	151	941	1967	4294	152	944	2082	4423
Timoshenko, elastic, analytical	138	867	1836	4115	138	868	1944	4158
Timoshenko, elastic, FEM	138	867	1837	4119	138	868	1943	4147
ANSYS (plane FE), elastic	141	889	1851	4077	142	891	1956	4200

5 Experiments—natural frequencies

Two different tests are performed on the delaminated unidirectional specimens: the modal hammer (or impact hammer) test and the sweep excitation test. Further details of the experiments can be found in [46,47]. The experiments are repeated in this paper for the sake of completeness. For unidirectional composite beams, the reference plane coordinates are given in Table 3. The further geometrical data are listed in Table 4.

6 Results and discussion

In this section, the first four natural frequencies by the analytical and finite element models are presented and compared to experimentally measured frequencies and also to those by the ANSYS plane FE model. Moreover, the displacement parameters and stress resultants are discussed. In the final subsection, the dynamic buckling phenomenon and the related stability diagrams as well as the critical forces and amplitudes are determined and commented.

6.1 Natural frequencies by models and experiments

The natural frequencies for sixteen different beam configurations are presented by the following models:

- Euler–Bernoulli beam theory, rigidly fixed end, analytical model [46] and FE solution [47] (note that this model can be obtained by using the Timoshenko beam model with $G_{12}=\infty$),
- Euler–Bernoulli beam theory, elastic foundation effect, analytical model and FE solution (using the Timoshenko beam model with $G_{12}=\infty$),
- Timoshenko beam theory, rigidly fixed end, analytical model developed in Sect. 2 and solved by Eq. (28) and FE solution detailed in section 3,
- Timoshenko beam theory, elastic foundation effect, analytical model developed in Sect. 2 and solved in accordance with Eq. (28) and FE solution developed in Sect. 3.

Table 6 presents the natural frequencies for the 60/0 and the 60/2 beams. It is observable right away that as the model is refined the values of frequencies get closer and closer to the measured values. As a matter of fact, the first effect is transverse shear, which is not considered by the Euler–Bernoulli beam theory. Comparing the results of the two theories from this point of view, it can be recognized that the effect of transverse shear is very small on the first frequency and moderate on higher frequencies. The second effect is the Winkler foundation

Table 7 Free vibration frequencies of the (60/4) and (60/6) composite beams with built-in+free ends in [Hz]

Beam configuration Frequencies	60/4				60/6			
	f_1	f_2	f_3	f_4	f_1	f_2	f_3	f_4
Modal hammer test	130	836	2041	4083	130	840	2192	4360
Sweep excitation test	124	824	2050	4080	126	834	2206	4390
E.-B., rigid, analytical	153	959	2389	5000	153	963	2610	5203
E.-B., rigid, FEM	153	959	2390	5005	154	963	2615	5220
E.-B., elastic, analytical	142	892	2230	4659	143	894	2425	4825
E.-B., elastic, FEM	142	891	2231	4667	143	894	2429	4841
Timoshenko, rigid, analytical	152	938	2293	4622	153	942	2489	4775
Timoshenko, rigid, FEM	152	939	2292	4613	153	943	2494	4788
Timoshenko, elastic, analytical	138	861	2132	4322	139	862	2304	4456
Timoshenko, elastic, FEM	138	861	2131	4313	139	863	2308	4466
ANSYS (plane FE), elastic	142	884	2158	4392	143	887	2360	4553

that the built-in length is resting on. A significant decrease in frequencies is clearly observable considering the Euler–Bernoulli beam models. This tendency further goes on by taking the results of the Timoshenko beam model into account. The explanation of the decrease in first frequency from 151 to 138 Hz in the latter case is the interaction between the transverse shear and elastic foundation effects. The elastic foundation represents the transverse elasticity of the built-in length, and thus, the stiffness of the system decreases compared to the rigidly fixed models. The degree of decrease results in the fact that the agreement between the first two and the last before rows in Table 6 becomes very good for all of the frequencies.

It was recognized that the sweep excitation test provides always a lower value for the first frequency than the modal hammer test. Considering the other frequencies, no clear tendencies were observed regarding the relationship (which one is higher or smaller); however, the values by the two methods are very close to each other.

The plane stress ANSYS FE model including the built-in length of the beams seems to agree very well with the Euler–Bernoulli model with elastic foundation effect if the first two frequencies are investigated. The third and fourth frequencies by the ANSYS model agree rather with the Timoshenko model dealing with the elastic foundation effect. Nevertheless, the definite agreement between the frequencies by the developed beam models and those by the ANSYS plane FE ones validates the former. This holds for any of the forthcoming tables.

The results of the 60/4 and 60/6 beams are summarized in Table 7. The tendencies and the relations of the analytical models and the experiments are likewise in the case of Table 6. For both Tables 6 and 7, the agreement between the analytical models and the corresponding FE models is excellent: there are only slight mismatches and essentially only the fourth frequency involves larger absolute differences. These small mismatches are dedicated to the different solution algorithms (bisection root finding vs. eigenvalue calculation).

The results of the 80/0, 80/2 and 80/4, 80/6 beams are collected in Tables 8 and 9. These results support the previous conclusions and observations; however, the agreement between the last before line and the first two ones is even better than in Tables 6 and 7. The difference between the analytical (or FE) models and the experiments is associated with the possible manufacturing defects. The final conclusion is that it is very important to apply an appropriate model to capture the reality and get consistent result. Some more tables are presented for the 100/0-100/6 and 120/0-120/6 beams, these are placed in Appendix A. The same conclusions are maintained as those for Tables 6, 7, 8, 9.

6.2 Displacement parameters and stress resultants

In the subsequent part of this article, the results of the Timoshenko beam finite element model are presented if otherwise not stated. Each figure is created with a 1 mm vibration amplitude at the end of the beam. Fig. 5 presents the deflection and the angle of rotation along the beam length for the first two natural frequencies of the 100/4 beam. The main aspect highlighted that is the influence of elastic foundation. Although the deflections are almost the same, the mismatch between the angle of rotations by rigidly fixed and Winkler foundation models is more pronounced. The effect of elastic foundation is the most significant at the built-in cross section (i.e., at $x = 0$) and decreases subsequently till the free end. It can be seen that the artificial power parameter (p_0) works well and prevents any delamination opening during vibration.

Table 8 Free vibration frequencies of the (80/0) and (80/2) composite beams with built-in+free ends in [Hz]

Beam configuration	80/0				80/2			
	f_1	f_2	f_3	f_4	f_1	f_2	f_3	f_4
Modal hammer test	132	823	1558	3248	132	842	1637	3427
Sweep excitation test	124	812	1598	3324	126	836	1784	3588
E.-B., rigid, analytical	148	925	1819	3853	151	944	1960	4136
E.-B., rigid, FEM)	148	923	1816	3855	151	943	1957	4139
E.-B., elastic, analytical	138	875	1682	3642	141	889	1818	3902
E.-B., elastic, FEM	138	875	1681	3645	140	888	1817	3907
Timoshenko, rigid analytical	147	908	1770	3675	150	926	1902	3920
Timoshenko, rigid, FEM	147	908	1769	3680	150	925	1899	3911
Timoshenko, elastic, analytical	135	850	1626	3471	137	861	1753	3699
Timoshenko, elastic, FEM	135	850	1625	3476	137	861	1751	3690
ANSYS (plane FE), elastic	138	866	1655	3501	140	879	1777	3714

Table 9 Free vibration frequencies of the (80/4) and (80/6) composite beams with built-in+free ends in [Hz]

Beam configuration	80/4				80/6			
	f_1	f_2	f_3	f_4	f_1	f_2	f_3	f_4
Modal hammer test	134	857	1927	3832	132	853	2158	4245
Sweep excitation test	126	848	1954	4044	126	850	2160	4260
E.-B., rigid, analytical	155	971	2283	4712	154	965	2566	5111
E.-B., rigid, FEM	155	971	2283	4720	154	965	2569	5129
E.-B., elastic, analytical	144	907	2120	4418	143	896	2381	4753
E.-B., elastic, FEM	138	906	2121	4427	143	897	2385	4769
Timoshenko, rigid, analytical	155	951	2197	4400	154	944	2449	4709
Timoshenko, rigid, FEM	155	950	2196	4387	154	945	2453	4717
Timoshenko, elastic, analytical	140	876	2031	4135	139	865	2265	4403
Timoshenko, elastic, FEM	140	876	2030	4122	139	866	2268	4408
ANSYS (plane FE), elastic	144	898	2061	4170	143	889	2319	4488

The longitudinal displacement and the normal force are plotted in Fig. 6 again for the 100/4 beam including the first two natural frequencies. An immediate observation is that the longitudinal displacement of the rigidly fixed model has a relatively higher slope than that of the elastic foundation model. The normal force is determined by the derivative of the longitudinal displacement (refer to Eq.(10)). The first and most important outcome of this analysis is that the normal force along the delaminated region is constantly distributed. Another important finding of this study is that the normal force by elastic foundation model is higher by around 10 percent than the one by the rigidly fixed model at the same vibration amplitude if the system performs harmonic vibration by the first natural frequency. In the case of the second natural frequency, the two models predict almost the same normal force. For higher modes, the effect of elastic foundation on the normal force distribution is more and more negligible.

The stress resultants (total bending moment and total shear force) are displayed in Fig. 7 for the first two vibration frequencies, again for the 100/4 beam. Note, that the sum of bending moments ($M_{xt} + M_{xb}$) is shown and not sum of the equivalent bending moments [46], that is the reason for the discontinuity between the delaminated and intact beam parts. For the first two frequencies, it is clearly recognized that the moment by elastic foundation model is smaller by approximately 18 and 27 % at $x = 0$ than those by the rigidly fixed formulation. From the standpoint of shear force, Fig. 7 indicates that it goes up suddenly and reaches a maximum value close to $x = 0$. First, the shear force is the higher at a specified cross section along the built-in length. Second, the shear force by the FE solution is piecewise constant. Thus, even the analytical solution is plotted in Fig. 7 for the elastic foundation providing excellent agreement with the FE solution. The difference between the shear forces by the two formulations is significant even along the effective beam length.

The most important role out of the stress resultants is attributed to the normal force, because this is the one governing the dynamic buckling phenomenon during free vibration.

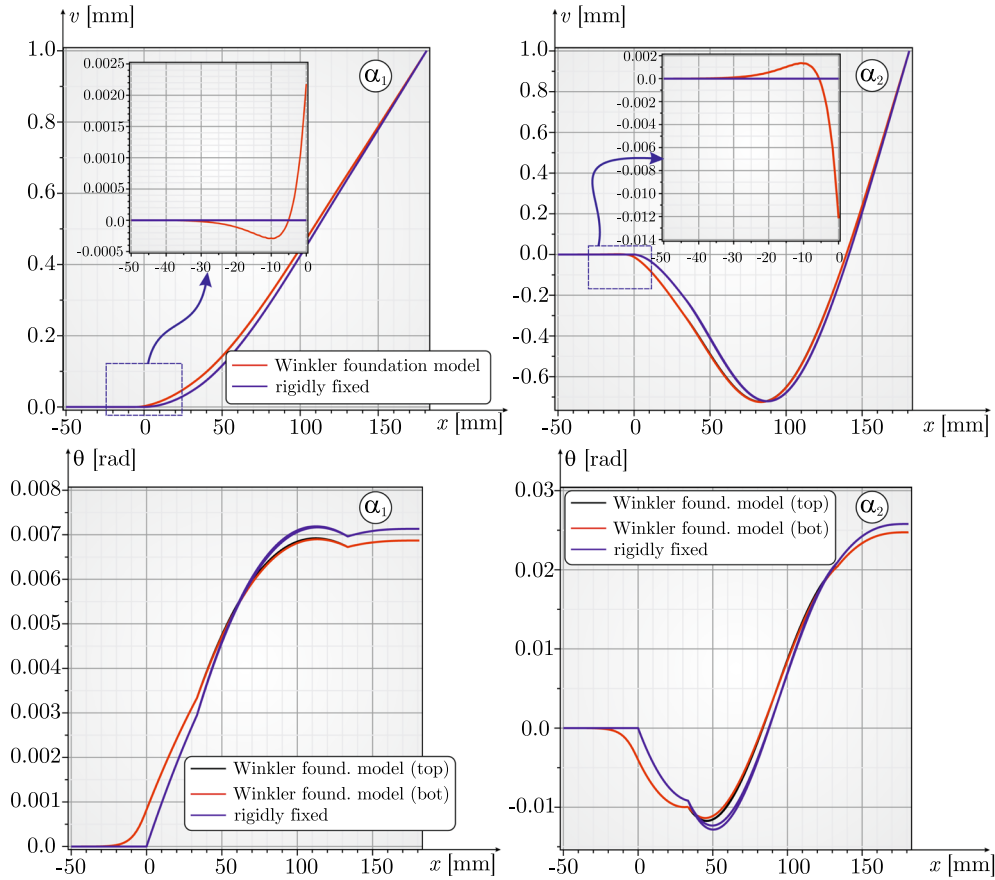


Fig. 5 Deflection and rotation along the length of the 100/4 beam for the first two vibration modes by rigid and elastic clamping

6.3 Dynamic buckling analysis

Figure 8 indicates how the parametric excitation takes place as the beam performs harmonic vibration. If the upward motion occurs, then the top beam is always compressed, the bottom is extended. If the downward motion is considered, then the top beam is extended and the bottom one is compressed. In other words, the tensile and compressive forces interchange each other with respect to the vibration frequency. It is important to recognize that the top beam can buckle only in the outward direction.

6.3.1 The geometric stiffness matrix

The buckling analysis requires the determination of the geometric stiffness matrix of the delaminated part for Euler-buckling. The strain energy from the nonlinear strain is [57]:

$$\mathcal{U}^{NL} = \int_V \sigma_x^0 \varepsilon^{NL} dV = \frac{1}{2} \mathbf{u}_e^T \mathbf{K}_{Ge} \mathbf{u}_e, \tag{63}$$

where the geometric stiffness matrix can be defined as:

$$\mathbf{K}_{Ge} = \int_{(V)} \mathbf{G}^T \mathbf{S} \mathbf{G} dV = \int_0^1 \frac{N}{l_e} \mathbf{N}'_v \mathbf{N}'_v{}^T d\xi, \tag{64}$$

where everything is determined for the top subbeam of the delaminated part using the Timoshenko beam model and N is the normal force distributed uniformly over the delamination length in accordance with Fig. 6. It has

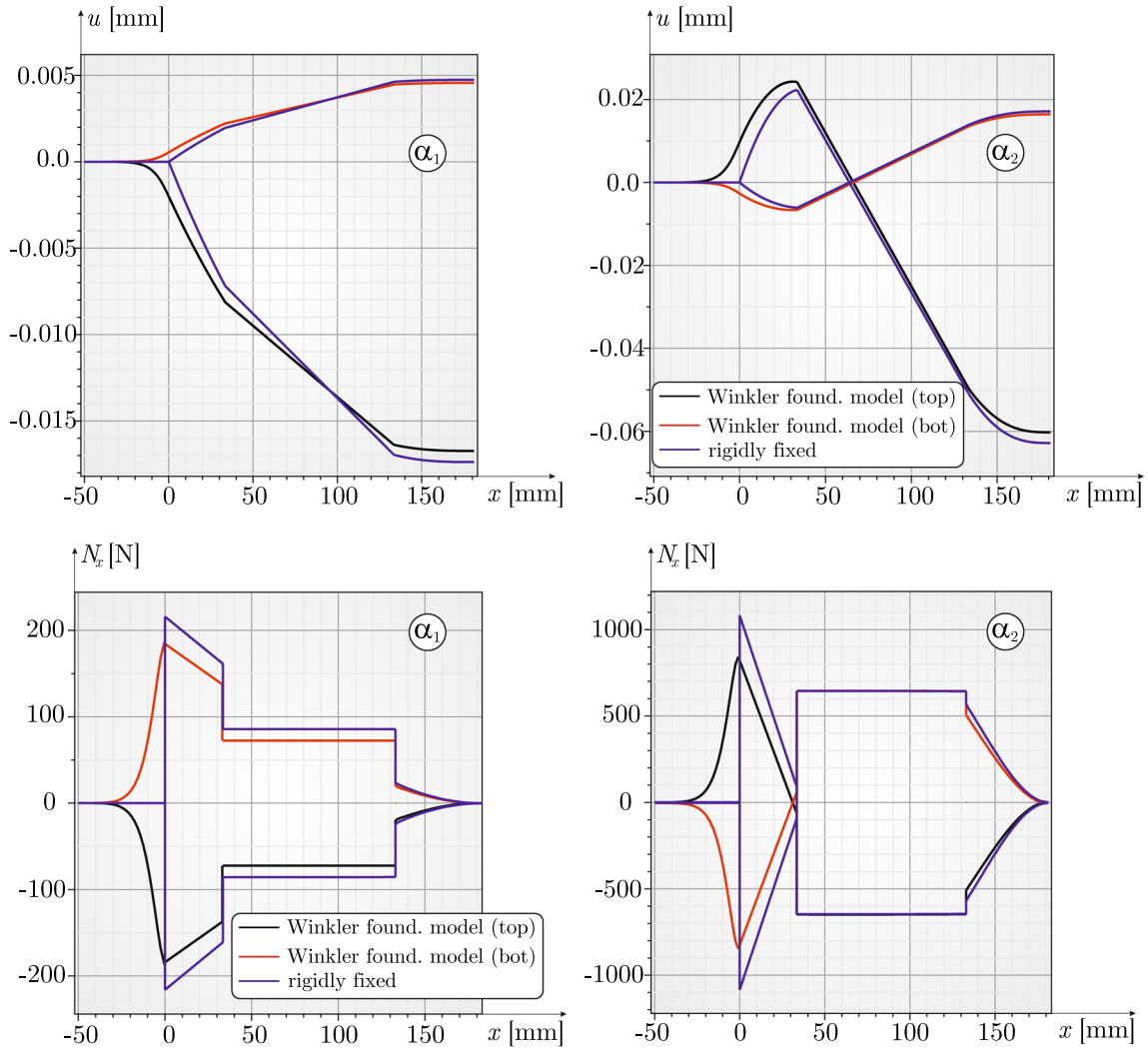


Fig. 6 Longitudinal displacement and normal force along the length of the 100/4 beam for the first two vibration modes

already been shown that the buckling takes place locally; thus, it is only investigated within the delaminated region.

6.3.2 The equation of motion and the solution

Let us consider only the top beam, the equation of motion has the following form [47]:

$$\mathbf{M}_t \ddot{\mathbf{U}}_t + \mathbf{K}_t \mathbf{U}_t + (F_d \mathbf{K}_{Gt}^0 \cos(\Theta t)) \mathbf{U}_t = \mathbf{0}, \quad (65)$$

where \mathbf{U}_t is the increment of the nodal displacement vector due to delamination buckling of the top subbeam, Θ is the frequency of parametric excitation; however, in this work, it will be one of the natural frequencies of the whole beam: $\Theta = \alpha$. The solution can be developed in accordance with [47]:

$$\mathbf{U}_t = \Phi \hat{T}(t), \quad (66)$$

where $\hat{T}(t)$ is the time function of the local delamination buckling having only a positive amplitude. This function can be expanded into a Fourier series and taken back into Eq. (65) [47]:

$$\mathbf{U}_t = \mathbf{a}_0 + \sum_{k=1,2,3,\dots}^{\infty} \mathbf{a}_k \cos(k\alpha t), \quad \mathbf{a}_0 = a_0 \Phi, \quad \mathbf{a}_k = a_k \Phi, \quad k = 1, 2, 3, \dots \quad (67)$$

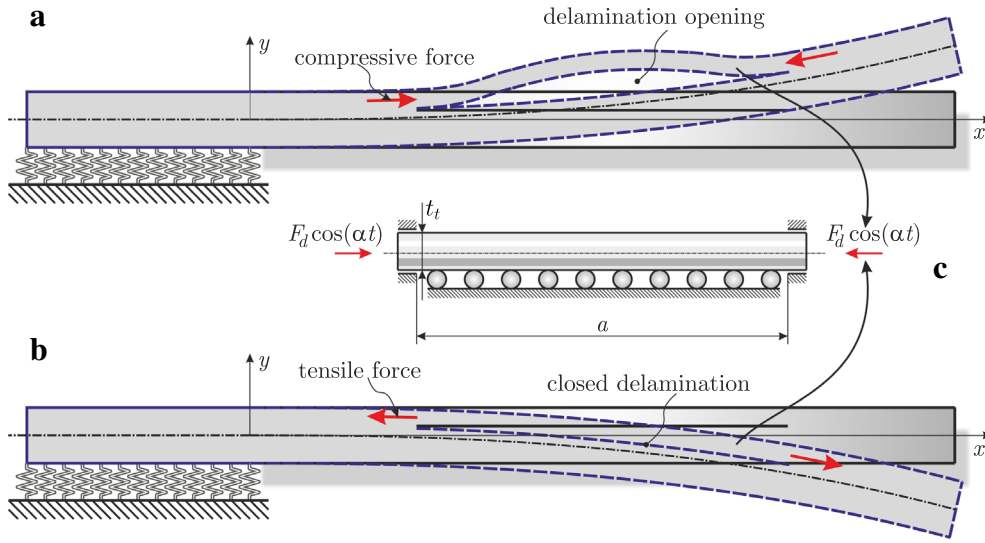


Fig. 8 The harmonically changing normal force in a delaminated beam under free vibration. Upward motion—compressive force (a), downward motion—tensile force (b). Local model of the parametrically excited top subbeam (c)

The determinant above leads to a lengthy two-variable function including the frequency and the force amplitude. Eq.(69) is called the general solution of the dynamic stability problem.

The second solution is based on the modal decomposition of the equation of motion. By multiplying the equation of motion by Φ (eigenmode vector of static buckling) from the left and right hand sides, the following scalar equation is obtained:

$$\ddot{\hat{T}}(t) + \Omega^2(1 + 2\mu \cos \alpha t)\hat{T}(t) = 0, \tag{70}$$

where:

$$\Omega = \frac{\Phi^T \mathbf{K}_t \Phi}{\Phi^T \mathbf{M}_t \Phi}, \quad \mu = \frac{1}{2} \frac{1}{\Omega^2} \frac{\Phi^T \mathbf{K}_{Gt} \Phi}{\Phi^T \mathbf{M}_t \Phi}. \tag{71}$$

The same procedure [47] as we have seen before to obtain Eq.(69) leads to the determinant below:

$$\begin{vmatrix} \Omega^2 & \Omega^2 \mu & 0 & 0 & 0 & \dots \\ 2\Omega^2 \mu & \Omega^2 - \alpha^2 & \Omega^2 \mu & 0 & 0 & \dots \\ 0 & \Omega^2 \mu & \Omega^2 - 4\alpha^2 & \Omega^2 \mu & 0 & \dots \\ 0 & 0 & \Omega^2 \mu & \Omega^2 - 9\alpha^2 & \Omega^2 \mu & \dots \\ 0 & 0 & 0 & \Omega^2 \mu & \Omega^2 - 16\alpha^2 & \dots \\ \vdots & \vdots & \vdots & \vdots & \vdots & \ddots \end{vmatrix} = 0. \tag{72}$$

As it can be seen in this case, the elements within the determinant are scalar parameters. However, the vector Φ should be determined for each delamination length and t_t thickness separately. In the sequel, we present the results of the dynamic stability analysis using both models (Eq. (69) and Eq. (72)). In each case, the matrices are determined by the Timoshenko beam finite element model Table 11.

6.4 Dynamic stability analysis results

This subsection is divided into two parts: one related to the determination of the critical value of the force and another dedicated to the critical amplitude of the free vibration.

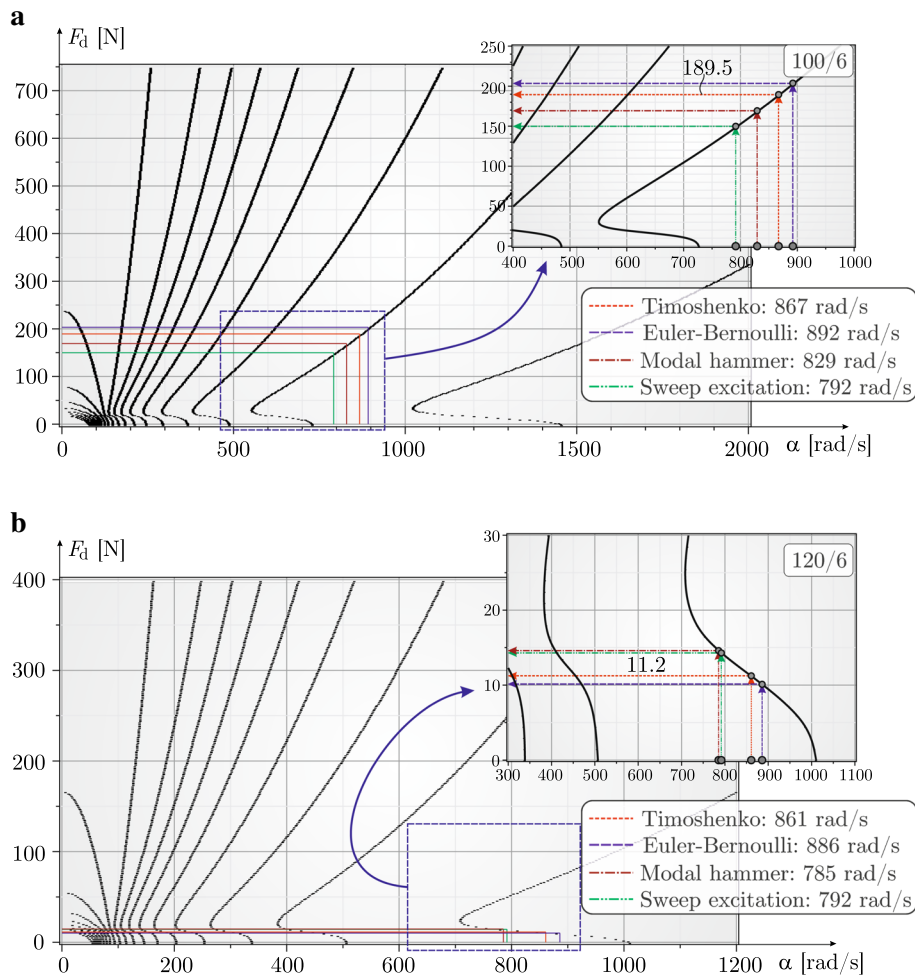


Fig. 9 Stability diagrams for local dynamic buckling of the 100/6 (a) and 120/6 (b) beams using the modal decomposition technique, $N_e=20$, $N_{det}=20$

6.4.1 Determination of the critical value of dynamic force

Figure 9 provides the stability diagram plots of the 100/6 and the 120/6 beams using the modal decomposition technique. Twenty (N_e) elements are applied along the length, and the twentieth-order determinant (N_{det}) is calculated. The convergence of the solution was investigated as well, and these parameters were found to be appropriate. The critical values of the dynamic force amplitude, F_d are shown against the natural frequency, the curves are determined by Eq. (72). The values of the first natural frequency by Timoshenko and Euler–Bernoulli beam theories including the Winkler foundation together with the modal hammer and sweep excitation tests are also shown with the corresponding force values. The enlarged subfigures on the right top corner show how the intersection and projection is performed in order to obtain the critical dynamic force amplitude. A detailed description of this procedure is given below:

- The first step is that we choose the theory or method the frequency is determined by. Let it be the Timoshenko beam theory. In Table 12, the first free vibration frequency of the 100/6 beam is 138 Hz by the Timoshenko beam theory including the elastic foundation effect (Tables 13, 14).
- Convert the former frequency to rad/s, this provides 867 rad/s.
- In order to find the critical value of the force, F_d indicated in Fig. 8 we consider Fig. 9. We find the first intersection between the solution curve and the vertical line going across the frequency value of 867 rad/s.
- The critical value of the force is determined by a horizontal line going across the intersection point, leading to 189.5 N as it can be seen in Fig. 9 as well.

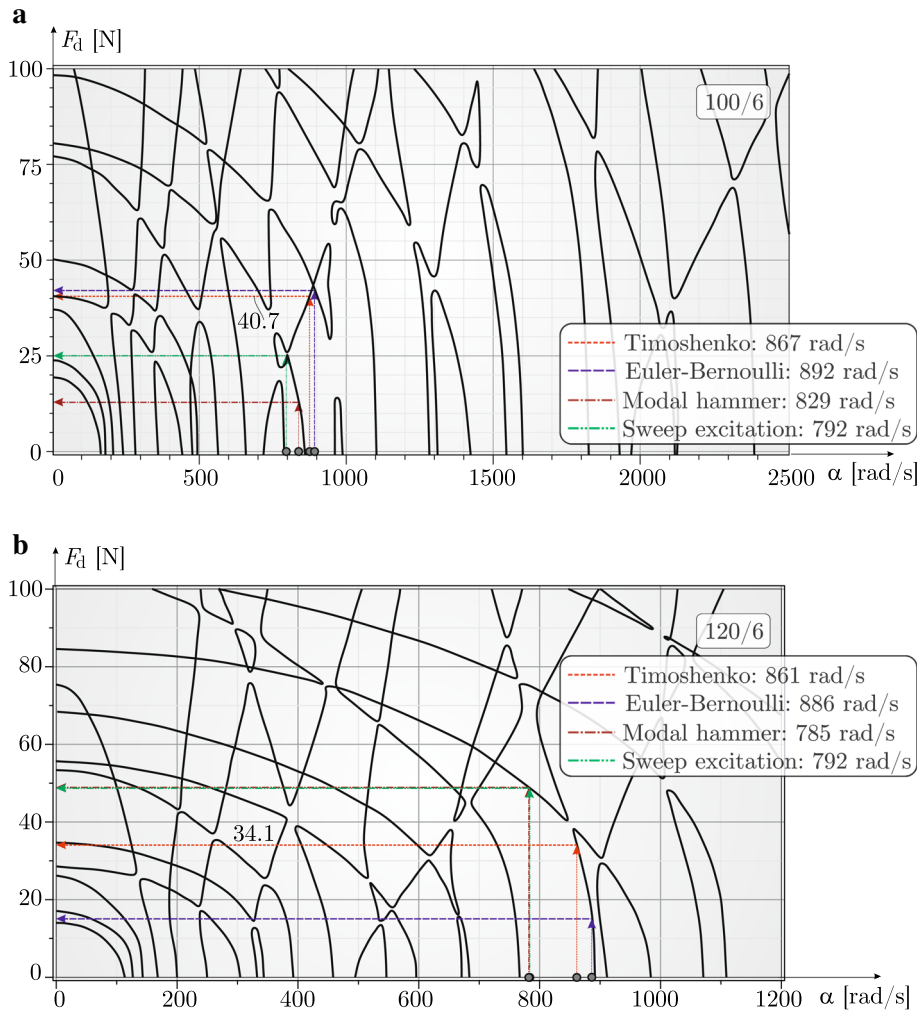


Fig. 10 Stability diagrams for local dynamic buckling of the 100/6 (a) and 120/6 (b) beams using the general solution, $N_e=12$, $N_{det}=10$

- The same procedure can be applied to any other frequency in order to determine the corresponding critical force. A consequence is that the critical value of the dynamic force is frequency dependent.

For both Figs. 9a, b, it can be recognized that the critical force amplitude is quite sensitive to the frequency. For the 100/6 beam, the first natural frequency by the Timoshenko, Euler–Bernoulli beam models and modal hammer test and the sweep excitation test intersects the same limit curve. However, it is possible that any of the former four frequencies—being a slightly smaller or greater than the other three—intersects with another limit curve resulting in a significantly smaller or larger critical force amplitude. The picture is quite similar to this if we take a look at Fig. 9b for the 120/6 beam.

Figure 10 presents the diagrams using the general description of the dynamic stability problem (Eq. (69)). In this case, both N_e and N_{det} are reduced ($N_e=12$, $N_{det}=10$) because of the significantly higher matrix size; however, convergence was again achieved in each investigated case. The first observation is that the picture by this general solution is quite different compared to that obtained by the modal decomposition technique related to Fig. 9. Nevertheless, the technique to determine the critical force amplitude is exactly the same. The frequencies for the 100/6 beam are given in the figure in rad/s and can be found in Table 12 in Hz. Based on the frequencies, the critical forces are easy to locate using the diagram. For both beam configurations, the limit curves in Figure 10 are again quite different than those in Fig. 9. In Fig. 10a, the critical force values are relatively close to each other; however, there is a huge mismatch with the forces in Fig. 9a (100/6 beam). For the 120/6 beam, the mismatch between Figs. 9b and 10b is again significant from the standpoint of critical

Table 10 Critical dynamic force values and critical vibration amplitudes by Timoshenko beam theory and experiment

Beam code	Model type	Continuum model		Modal decomposition		General solution		Experiment δ_{exp} [mm]
		f_1 [Hz]	N_{xt} [N]	F_d [N]	δ_{cr} [mm]	F_d [N]	δ_{cr} [mm]	
60/6	Rigid	153	32.8	29.3	0.89	35.2	1.07	0.46
	Elastic	139	27.0	53.3	1.97	79.7	2.95	
80/6	Rigid	154	33.8	29.3	0.87	50.7	1.50	0.3
	Elastic	139	28.3	39.2	1.39	14.1	0.50	
100/6	Rigid	152	35.7	39.5	1.11	25.6	0.72	0.12
	Elastic	138	29.9	189.5	6.33	40.7	1.36	
120/6	Rigid	151	35.6	7.0	0.2	19.3	0.54	0.04
	Elastic	137	29.9	11.2	0.38	34.1	1.14	

forces; however, the solution is definitely more sensitive to the frequency by the general solution because of the relatively large slope of the curves.

In order to elaborate how the thicknesswise position of the delamination influences the stability diagrams, we provide Figs. 11 and 12. In Fig. 11, the results by the modal decomposition technique are plotted for the 100/0, 100/2 and 100/4 beams, respectively. Obviously, relatively huge values are obtained for the dynamic force amplitude in each case. This can be explained by the fact that the slope of the curves becomes higher and higher. The general solution provides the curves in Figs. 12a–c; the sensitivity of the critical dynamic force to the frequency is still brought to the stage by these results.

Here, an alternative utilization of the results in Figs. 9, 10, 11, 12 is explained. The dynamic stability analysis is carried out by taking only the top beam of the delaminated part into consideration (local model, refer to Figure 8). Therefore, the surrounding structure of this top beam is no longer required to obtain the critical force values. The conclusion is that if in any (fictitious) structure the delaminated part has the same geometry and material as that Figs. 9, 10, 11, 12 are determined based on, then the presented figures remain true even for this structure. Once the frequencies of this fictitious structure are determined, we know the frequency of parametric excitation and we can determine the critical force, too.

6.4.2 Determination of the critical vibration amplitude

In this work, the Timoshenko beam model without and with built-in length resting on Winkler elastic foundation is chosen to determine the critical amplitudes required to initiate dynamic buckling. The modal decomposition technique as well as the general solution are applied to both models. The structure of Table 10 is the following. The results of the continuum model, i.e., the numerical FE model (they give the same results) are collected in the third and fourth columns for the .../6 beams. These results are the first natural frequency and the normal force at the left crack tip (which is uniform along the delaminated part). The subsequent columns contain the critical values of the F_d force amplitude (detailed in the previous subsection) and the critical vibration amplitude. The latter is always the ratio of F_d over N_{xt} . The critical amplitudes were also determined experimentally in a previous work [47]; these values are listed in the last column of Table 10. The comparison of the critical vibration amplitudes from the models and by experiments shows that the agreement is bad. The biggest discrepancy takes place for the 100/6 beam by the elastic foundation model combined with the modal decomposition technique providing a critical vibration amplitude of 6.33 mm against the 0.12 mm value by experiment. Overall, it seems that in spite of the fact that the modal decomposition technique seems to be justified, the general solution is free of extreme discrepancies compared to the experiments. We highlight again the sensitivity of the force amplitude to the frequency, which is the main reason for the mismatches between model prediction and experiments. Also, in a previous work the agreement between the critical vibration amplitudes by the Euler–Bernoulli model without elastic foundation and by experiments was better. The reason for this is that based on Fig. 9 lower dynamic force amplitudes are associated with the higher frequencies, and based on Tables 6, 7, 8, 9 the Euler–Bernoulli model without the elastic foundation results in the highest natural frequencies.

7 Conclusions

In this paper, the dynamics of delaminated composite beams was investigated using the Timoshenko and Euler–Bernoulli beam theories. The work was done essentially in two different aspects. In the first phase, the

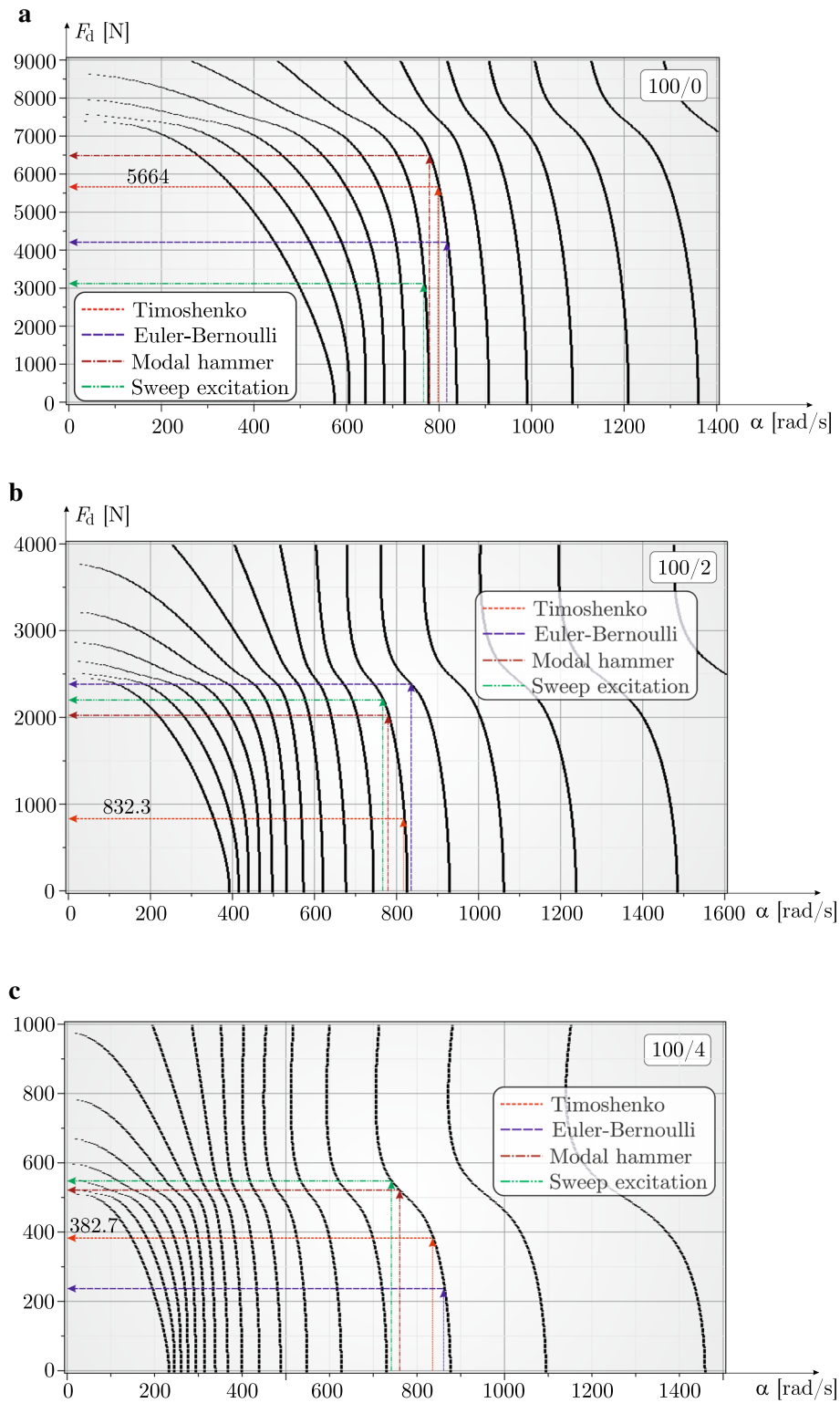


Fig. 11 Stability diagrams for local dynamic buckling of the 100/0 (a), 100/2 (b) and 100/4 (c) beams using the modal decomposition technique, $N_e=20$, $N_{det}=20$

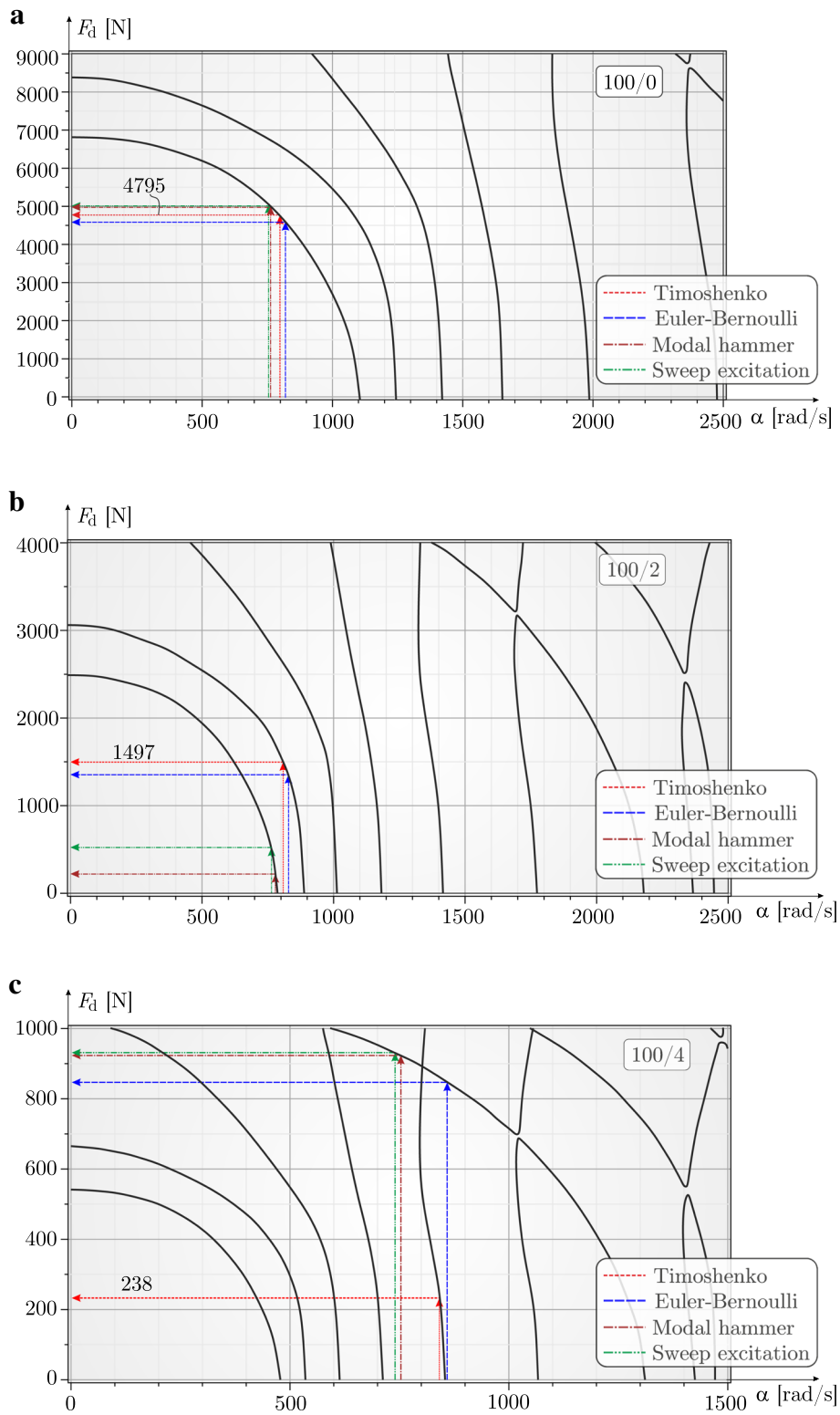


Fig. 12 Stability diagrams for local dynamic buckling of the 100/0 (a), 100/2 (b) and 100/4 (c) beams using the general solution, $N_e=12$, $N_{det}=10$

free vibration of the clamped beams was investigated using two different models. The built-in length of the model was captured by the Winkler type elastic foundation providing an additional transverse displacement and rotation compared to the rigidly fixed case. The analysis was carried out by developing the governing differential equations for every regions of the beam and by solving the equations analytically. Also, the numerical solution was provided by the finite element method. The natural frequencies, mode shapes and the stress resultants were determined in the first phase of the work. The natural frequencies were determined also by experiments using modal hammer and sweep excitation tests. The comparison of analytical and experimental results showed that the Timoshenko beam theory with elastic foundation along the built-in length provides the best agreement with the measured frequencies. Note, that the first four natural frequencies were compared to each other.

In the second phase, the dynamic buckling phenomenon was investigated using the harmonic balance method. Two different approximations were applied. The general description is based on a determinant of a matrix with matrix elements. This approximation was also applied in a previous paper [47]. The second solution is based on the modal decomposition technique providing a quite similar determinant of a matrix; however, the latter contained scalar terms only. The stability limit curves of dynamic buckling in the plane of the free vibration frequency and the dynamic force amplitude were determined by both approximations. The critical dynamic forces were determined for the frequencies by Timoshenko beam theory, Euler–Bernoulli beam theory (both involved the effect of elastic foundation), moreover, for the frequencies by modal hammer and sweep excitation tests, respectively. The results indicated that the critical dynamic force is quite sensitive to the frequency. Thus, the agreement between the theoretical and experimental critical vibration amplitudes at which the buckling initiates was bad. However, the models developed in this work made it clear that the phenomenon itself is more complex than it was thought before and neither of the previous works revealed this feature of the free vibration problem of delaminated composite beams in the past.

The next step should be to elaborate how the damping affects the stability curves. Apparently, damping has a negligible effect on the natural frequencies but has a substantial effect on the stability curves of parametrically excited systems [50]. Nevertheless, being a special case investigated in this paper it is still an unsolved problem.

Acknowledgements This work has been supported by the National Research, Development and Innovation Office (NKFI) under grant No.134303. The research reported in this paper and carried out at BME has been supported by the NRDI Fund (TKP2020 IES, Grant No. BME-IE-NAT) based on the charter of bolster issued by the NRDI Office under the auspices of the Ministry for Innovation and Technology.

Funding Open access funding provided by Budapest University of Technology and Economics.

Compliance with ethical standards

Conflict of interest The author declares that he has no conflict of interest.

Open Access This article is licensed under a Creative Commons Attribution 4.0 International License, which permits use, sharing, adaptation, distribution and reproduction in any medium or format, as long as you give appropriate credit to the original author(s) and the source, provide a link to the Creative Commons licence, and indicate if changes were made. The images or other third party material in this article are included in the article's Creative Commons licence, unless indicated otherwise in a credit line to the material. If material is not included in the article's Creative Commons licence and your intended use is not permitted by statutory regulation or exceeds the permitted use, you will need to obtain permission directly from the copyright holder. To view a copy of this licence, visit <http://creativecommons.org/licenses/by/4.0/>.

Appendix A - Natural frequencies of the 100/0-100/6 and 120/0-120/6 beams

Table 11 Free vibration frequencies of the (100/0) and (100/2) composite beams with built-in+free ends in [Hz]

Beam configuration	100/0				100/2			
	f_1	f_2	f_3	f_4	f_1	f_2	f_3	f_4
Modal hammer test	124	738	1396	2842	124	756	1511	3000
Sweep excitation test	122	766	1640	3084	122	762	1644	3104
E.-B., rigid, analytical	138	831	1701	3444	142	857	1841	3716
E.-B., rigid, FEM	138	831	1702	3453	142	856	1836	3714
E.-B., elastic, analytical	130	803	1565	4418	133	822	1770	3447
E.-B., elastic FEM	130	803	1564	4427	133	822	1771	3449
Timoshenko, rigid, analytical	138	820	1664	3304	141	844	1789	3535
Timoshenko, rigid, FEM	138	820	1661	3306	141	842	1784	3527
Timoshenko, elastic, analytical	127	786	1510	3057	130	802	1627	3281
Timoshenko, elastic, FEM	127	786	1508	3061	130	802	1623	3276
ANSYS (plane FE), elastic	130	793	1550	3123	132	810	1664	3332

Table 12 Free vibration frequencies of the (100/4) and (100/6) composite beams with built-in+free ends in [Hz]

Beam configuration	100/4				100/6			
	f_1	f_2	f_3	f_4	f_1	f_2	f_3	f_4
Modal hammer test	121	781	1692	3532	132	854	2135	4125
Sweep excitation test	118	754	1726	3524	126	850	2136	4144
E.-B., rigid, analytical	147	902	2123	4259	152	950	2513	4963
E.-B., rigid, FEM	147	901	2120	4264	152	950	2516	4980
E.-B., elastic, analytical	137	851	1958	3969	142	885	2327	4611
E.-B., elastic, FEM	137	851	1958	3975	142	886	2330	4626
Timoshenko, rigid, analytical	137	851	1958	3969	152	930	2402	4586
Timoshenko, rigid, FEM	137	851	1958	3975	152	931	2404	4594
Timoshenko, elastic, analytical	133	826	1878	3740	138	856	2214	4284
Timoshenko, elastic, FEM	133	826	1875	3731	138	856	2217	4290
ANSYS (plane FE), elastic	136	841	1915	3784	142	878	2270	4365

Table 13 Free vibration frequencies of the (120/0) and (120/2) composite beams with built-in+free ends in [Hz]

Beam configuration	120/0				120/2			
	f_1	f_2	f_3	f_4	f_1	f_2	f_3	f_4
Modal hammer test	122	686	1487	2838	120	705	1527	2905
Sweep excitation test	120	720	1534	2914	118	724	1592	3024
E.-B., rigid, analytical	129	754	1620	3272	135	800	1759	3533
E.-B., rigid, FEM	129	754	1613	3267	135	798	1752	3528
E.-B., elastic, analytical	122	737	1500	3035	127	774	1625	3258
E.-B., elastic, FEM	122	736	1499	3038	127	774	1624	3257
Timoshenko, rigid, analytical	129	746	1585	3136	135	789	1716	3368
Timoshenko, rigid, FEM	129	746	1581	3136	135	787	1708	3359
Timoshenko, elastic, analytical	120	725	1454	2886	125	759	1571	3102
Timoshenko, elastic, FEM	120	724	1450	2887	125	758	1565	3095
ANSYS (plane FE), elastic	122	726	1491	2969	127	762	1608	3176

Table 14 Free vibration frequencies of the (120/4) and (120/6) composite beams with built-in+free ends in [Hz]

Beam configuration Method, theory	120/4				120/6			
	f_1	f_2	f_3	f_4	f_1	f_2	f_3	f_4
Modal hammer test	130	715	1889	3749	125	857	2182	4144
Sweep excitation test	122	794	1872	3694	126	836	2148	4086
E.-B., rigid, analytical	144	868	2071	4118	151	938	2485	4887
E.-B., rigid, FEM	144	867	2066	4120	151	938	2486	4902
E.-B., elastic, analytical	134	826	1911	3804	141	877	2299	4524
E.-B., elastic, FEM	134	826	1912	3808	141	877	2302	4538
Timoshenko, rigid, analytical	143	853	2003	3876	151	919	2377	4521
Timoshenko, rigid, FEM	143	852	1995	3864	151	919	2377	4527
Timoshenko, elastic, analytical	131	805	1837	3589	137	848	2190	4208
Timoshenko, elastic, FEM	131	804	1831	3580	137	849	2191	4214
ANSYS (plane FE), elastic	134	815	1878	3657	141	869	2245	4293

References

- Ramkumar, R.L., Kulkarni, S.V., Pipes, R.B.: "Free vibration frequencies of a delaminated beam," in *34th Annual Technical Conference*, no. 22-E, pp. 1–5, Reinforced Plastics/Composites Institute, The Society of the Plastic Industry, (1979)
- Mujumdar, P., Suryanarayan, S.: Flexural vibration of beams with delaminations. *J. Sound Vib.* **125**(3), 441–461 (1988)
- Tracy, J., Pardoan, G.: Effect of delamination on the natural frequencies of composite laminates. *J. Compos. Mater.* **23**(12), 1200–1215 (1989)
- Shu, D., Fan, H.: Free vibration of bimaterial split beam. *Compos. Part B - Eng.* **27B**, 76–84 (1996)
- Shu, D.: Vibration of sandwich beams with double delaminations. *Compos. Sci. Technol.* **54**, 101–109 (1995)
- Lee, J.: Free vibration analysis of delaminated composite beams. *Comput. Struct.* **74**, 121–129 (2000)
- Wang, J., Tong, L.: A study of the vibration of delaminated beams using a nonlinear anti-interpenetration constraint model. *Compos. Struct.* **57**(1–4), 483–488 (2002)
- Shu, D., Della, C.N.: Vibrations of multiple delaminated beams. *Compos. Struct.* **64**, 467–477 (2004)
- Mahieddine, A., Pouget, J., Ouali, M.: Modeling and analysis of delaminated beams with integrated piezoelectric actuators. *Compt. Rendus - Mecanique* **338**(5), 283–289 (2010)
- Mahieddine, A., Ouali, M.: Modeling and analysis of beams with delamination. *Int. J. Model. Simul. Sci. Comput.* **1**(3), 435–444 (2010)
- Çallioğlu, H., Atlıhan, G.: "Vibration analysis of delaminated composite beams using analytical and FEM models," *Indian J. Eng. Mater. Sci.*, vol. 18, pp. 7–14, (2011)
- Çallioğlu, H., Atlıhan, G., Topçu, M.: "Vibration analysis of multiple delaminated composite beams," *Adv. Compos. Mater.*, vol. 21, no. 1, pp. 11–27, (2012)
- Kargarnovin, M.H., Ahmadian, M.T., Jafari-Talookolaei, R.A.: Forced vibration of delaminated Timoshenko beams subjected to a moving load. *Sci. Eng. Compos. Mater.* **19**(2), 145–157 (2012)
- Manoach, E., Warminski, J., Mitura, A., Samborski, S.: Dynamics of a composite Timoshenko beam with delamination. *Mech. Res. Commun.* **46**, 47–53 (2012)
- Li, S., Fan, L.: Free vibration of FGM Timoshenko beams with through-width delamination. *Sci. Chin. Phys. Mech. Astron.* **57**(5), 927–934 (2014)
- Jafari-Talookolaei, R.-A., Abedi, M.: "Analytical solution for the free vibration analysis of delaminated Timoshenko beams," *Sci. World J.*, 2014. Article ID: 280256
- Pölöskei, T., Szekrényes, A.: Dynamic stability analysis of delaminated composite beams in frequency domain using a unified beam theory with higher order displacement continuity. *Compos. Struct.* **272**, 114173 (2021)
- Shen, M.-H., Grady, J.: Free vibrations of delaminated beams. *AIAA J.* **30**(5), 1361–1370 (1992)
- Kargarnovin, M.H., Ahmadian, M.T., Jafari-Talookolaei, R.A., Abedi, M.: Semi-analytical solution for the free vibration analysis of generally laminated composite Timoshenko beams with single delamination. *Compos. Part B: Eng.* **45**(1), 587–600 (2013)
- Luo, H., Hanagud, S.: Dynamics of delaminated beams. *Int. J. Solids Struct.* **37**, 1501–1519 (2000)
- Shu, D., Della, C.N.: Free vibration analysis of composite beams with overlapping. *Eur. J. Mech. A/Solids* **24**, 491–503 (2005)
- Lee, S., Park, T., Voyiadjis, G.Z.: Vibration analysis of multi-delaminated beams. *Compos. Part B - Eng.* **34**, 647–659 (2003)
- Park, T., S Lee, A. G. Z. V.: "Recurrent single delaminated beam model for vibration analysis of multidelaminated beams," *J. Eng. Mech.*, vol. 130, no. 9, pp. 1072–1082, (2004)
- Perel, V.Y.: Finite element analysis of vibration of delaminated composite beam with an account of contact of the delamination crack faces, based on the first-order shear deformation theory. *J. Compos. Mater.* **39**(20), 1843–1876 (2005)
- Perel, V.Y.: A numerical-analytical solution for dynamics of composite delaminated beam with piezoelectric actuator, with account of nonpenetration constraint for the delamination crack faces. *J. Compos. Mater.* **39**(1), 67–103 (2005)
- Perel, V.Y.: A new approach for finite element analysis of delaminated composite beam, allowing for fast and simple change of geometric characteristics of the delaminated area. *Struct. Eng. Mech.* **25**(5), 501–508 (2007)
- Tang, H., Wu, C., Huang, X.: Vibration analysis of a coupled beam-sdof system by using the recurrence equation method. *J. Sound Vib.* **311**, 912–923 (2008)

28. Hu, N., Fukunaga, H., Kameyama, M., Aramaki, Y., Chang, F.: Vibration analysis of delaminated composite beams and plates using a higher-order finite element. *Int. J. Mech. Sci.* **44**, 1479–1503 (2002)
29. Chakraborty, A., Mahapatra, D.R., Gopalakrishnan, S.: Finite element analysis of free vibration and wave propagation in asymmetric composite beams with structural discontinuities. *Compos. Struct.* **55**, 23–26 (2002)
30. Torabi, K., Shariati-Nia, M., Heidari-Rarani, M.: Experimental and theoretical investigation on transverse vibration of delaminated cross-ply composite beams. *Int. J. Mech. Sci.* **115–116**, 1–11 (2016)
31. Jafari-Talookolaei, R.-A., Lasemi-Imani, S.: Free vibration analysis of a delaminated beam-fluid interaction system. *Ocean Eng.* **107**, 186–192 (2015)
32. Erdelyi, N.H., Hashemi, S.M.: “A dynamic stiffness element for free vibration analysis of delaminated layered beams,” *Modell. Simul. Eng.*, vol. Article ID 492415, 8 pages, (2012)
33. Shams, S., Torabi, A., Narab, M.F., Atashgah, M.A.: Free vibration analysis of a laminated beam using dynamic stiffness matrix method considering delamination. *Thin-Walled Struct.* **166**, 107952 (2021)
34. Alidoost, H., Rezaeepazhand, J.: Instability of a delaminated composite beam subjected to a concentrated follower force. *Thin-Walled Struct.* **120**, 191–202 (2017)
35. Sha, G., Cao, M., Radziński, M., Ostachowicz, W.: Delamination-induced relative natural frequency change curve and its use for delamination localization in laminated composite beams. *Compos. Struct.* **230**, 111501 (2019)
36. Barman, S.K., Maiti, D.K., Maity, D.: Vibration-based delamination detection in composite structures employing mixed unified particle swarm optimization. *AIAA J.* **59**(1), 386–399 (2021)
37. Burlayenko, V.N., Sadowski, T.: Influence of skin/core debonding on free vibration behavior of foam and honeycomb cored sandwich plates. *Int. J. Non-Linear Mech.* **45**(10), 959–968 (2010)
38. Burlayenko, V., Sadowski, T.: Dynamic behaviour of sandwich plates containing single/multiple debonding. *Comput. Mater. Sci.* **50**(4), 1263–1268 (2011)
39. Damanpack, A., Bodaghi, M.: A new sandwich element for modeling of partially delaminated sandwich beam structures. *Compos. Struct.* **256**, 113068 (2021)
40. Shahedi, S., Mohammadimehr, M.: Vibration analysis of rotating fully-bonded and delaminated sandwich beam with centre face sheets and aluminium-foam flexible core in thermal and moisture environments. *Mech. Based Design Struct. Machine.* **48**(5), 584–614 (2020)
41. Babu, A.A., Vasudevan, R.: Dynamic instability analysis of rotating delaminated tapered composite plates subjected to periodic in-plane loading. *Archive Appl. Mech.* **86**(12), 1965–1986 (2016)
42. Hirwani, C.K., Patil, R.K., Panda, S.K., Mahapatra, S.S., Mandal, S.K., Srivastava, L., Buragohain, M.K.: Experimental and numerical analysis of free vibration of delaminated curved panel. *Aerospace Sci. Technol.* **54**, 353–370 (2016)
43. Hirwani, C.K., Panda, S.K.: Nonlinear thermal free vibration frequency analysis of delaminated shell panel using FEM. *Compos. Struct.* **224**, 111011 (2019)
44. Hirwani, C.K., Panda, S.K., Patle, B.: Theoretical and experimental validation of nonlinear deflection and stress responses of an internally debonded layer structure using different higher-order theories. *Acta Mech.* **229**(8), 3453–3473 (2018)
45. Chen, J., Wang, H., Qing, G.: Modeling vibration behavior of delaminated composite laminates using meshfree method in Hamilton system. *Appl. Math. Mech.* **36**(5), 633–654 (2015)
46. Szekrényes, A.: Coupled flexural-longitudinal vibration of delaminated composite beams with local stability analysis. *J. Sound Vib.* **333**(20), 5141–5164 (2014)
47. Szekrényes, A.: A special case of parametrically excited systems: free vibration of delaminated composite beams. *Euro. J. Mech. A/Solids* **49**, 82–105 (2015)
48. Szekrényes, A.: Natural vibration-induced parametric excitation in delaminated Kirchhoff plates. *J. Compos. Mater.* **50**(17), 2337–2364 (2016)
49. Pölöskei, T., Szekrényes, A.: Quasi-periodic excitation in a delaminated composite beam. *Compos. Struct.* **159**, 677–688 (2017)
50. Pölöskei, T., Szekrényes, A.: “Dynamic stability of a structurally damped delaminated beam using higher order theory,” *Math. Problems Eng.*, vol. 2018, (2018)
51. Pölöskei, T., Szekrényes, A.: Dynamic stability analysis of reduced delaminated planar beam structures using extended Craig-Bampton method. *Appl. Math. Modell.* **102**, 153–169 (2022)
52. Reddy, J.N.: *Mechanics of laminated composite plates and shells - Theory and analysis*. Boca Raton, London, New York, Washington D.C.: CRC Press, (2004)
53. Chou, P.C., Pagano, N.J.: *Elasticity - Tensor, dyadic, and engineering approaches*. D. Van Nostrand Company Inc, Princeton, New Jersey, Toronto, London (1967)
54. Kollár, L., Springer, G.: *Mechanics of composite structures*. Cambridge University Press, Cambridge, New York, Melbourne, Madrid, Capetown, São Paulo (2002)
55. Kanninen, M.: An augmented double cantilever beam model for studying crack propagation and arrest. *Int. J. Fract.* **9**(1), 83–92 (1973)
56. Petyt, M.: *Introduction to Finite Element Vibration Analysis*. Cambridge, New York, Melbourne, Madrid, Cape Town, Singapore, São Paulo, Delhi, Dubai, Tokyo, Mexico City: Cambridge University Press, second ed., (2010)
57. Cook, R. D., Malkus, D. S., Plesha, M. E., Witt, R. J.: “Concepts and applications of finite element analysis,” *New York*, (1989)
58. Reddy, J.N.: On the dynamic behaviour of the Timoshenko beam finite elements. *Sadhana* **24**(3), 175–198 (1999)
59. Friedman, Z., Kosmatka, J.B.: An improved two-node Timoshenko beam finite element. *Comput. Struct.* **47**(3), 473–481 (1993)
60. Bolotin, W.W.: *Kinetische Stabilität Elastischer Syst.* VEB Deutscher Verlag der Wissenschaften, Berlin (1961)